



---

# Localization of the Acoustic Center for the Holographic Measurement of Loudspeaker

---

Yuyang LIU

Yuyang.Liu.Etu@univ-lemans.fr

**Supervisor :** Christian BELLMANN  
**Academic Referee :** Antonin NOVAK

Klippel GmbH

Le Mans Université

International Master's Degree in ElectroAcoustics

3 September 2024

Not Confidential

## Acknowledgment

I would like to express my deepest gratitude to everyone who supported me throughout this project.

First and foremost, I would like to thank Le Mans University and IMDEA for offering the internship program, and Klippel GmbH for allowing me to carry out my master's thesis internship at their company. It has been an invaluable experience that has greatly contributed to my growth. I truly cherish every day I spent at Klippel GmbH, along with every outstanding colleague I had the pleasure to meet. I am also grateful for the financial support provided by the IA-GS Scholarship and the Erasmus Scholarship, which ensured my well-being and allowed me to complete my internship and thesis successfully.

I would also like to extend my sincere thanks to Dipl.-Ing. Christian Bellmann for proposing the project topic and offering his invaluable support throughout the entire internship. His extensive experience, knowledge, and patient guidance were instrumental in the smooth progress of my work. The equal and friendly exchanges with Christian Bellmann deepened my understanding of the subject and fueled my passion for the project. I am equally thankful to Prof. Dr. Wolfgang Klippel for providing critical insights and ideas that significantly shaped my thesis, as well as to all colleagues who actively participated in discussions and contributed valuable suggestions.

Furthermore, I would like to express my appreciation to Dr. Antonin Novak for serving as the reviewer of my thesis. I am also grateful to all the faculty and students at IMDEA for their academic and personal support. It has been an honor to meet and progress alongside such wonderful people.

Moreover, I would like to extend my heartfelt thanks to everything and everyone I encountered in Dresden. I am especially grateful to my good friend, Baptiste Fourier, for his companionship at the company. I also want to thank all the friends I made in Germany, as well as the nature of Dresden, which allowed me to find solace and reflect on the meaning of life. I am deeply thankful to my family and friends in China for their constant care and concern from afar. Finally, I want to thank myself for growing stronger and more determined as I continue this journey with courage and conviction.

Lastly, thanks for the passion.

## List of Abbreviations

### Klippel Product & Module

|                     |                                     |
|---------------------|-------------------------------------|
| <b>QC</b>           | Quality Control                     |
| <b>LPM</b>          | Lumped Parameter Measurement        |
| <b>NFS</b>          | Near Field Scanner                  |
| <b>KA3</b>          | Klippel Analyzer 3                  |
| <b>KCS</b>          | Klippel Controlled Sound Technology |
| <b>KlAutomation</b> | Klippel Automation                  |

### Klippel NFS Operations

|            |                                  |
|------------|----------------------------------|
| <b>MDC</b> | Measurement Data Container       |
| <b>HFI</b> | Holographic Field Identification |

### Others

|             |  |
|-------------|--|
| <b>SW</b>   | Spherical Waves                            |
| <b>SHF</b>  | Spherical Harmonic Functions               |
| <b>BEM</b>  | Boundary Element Method                    |
| <b>LMS</b>  | Least Mean Square                          |
| <b>DALM</b> | Difference of Arrival Linearization Matrix |
| <b>WEM</b>  | Wave Expansion Based Method                |
| <b>TFE</b>  | Total Fitting Error                        |
| <b>API</b>  | Application Programming Interface          |
| <b>IR</b>   | Impulse Response                           |

# Contents

|          |   |           |
|----------|---|-----------|
| <b>1</b> | <b>Company Introduction</b>                                       | <b>1</b>  |
| <b>2</b> | <b>Project Context &amp; Aim</b>                                  | <b>1</b>  |
| 2.1      | System Under Study - Klippel Near Field Scanner . . . . .         | 1         |
| 2.2      | Necessity of Acoustic Center Localization . . . . .               | 2         |
| <b>3</b> | <b>Work Constraint</b>  | <b>3</b>  |
| <b>4</b> | <b>Litterature Review</b>   | <b>3</b>  |
| <b>5</b> | <b>Theory Framework</b>   | <b>6</b>  |
| 5.1      | Simulated Sound Field . . . . .                                   | 6         |
| 5.2      | Delay Method . . . . .  | 7         |
| 5.2.1    | Group Delay . . . . .   | 7         |
| 5.2.2    | LMS Algorithm . . . . .   | 8         |
| 5.2.3    | DALM Algorithm . . . . .  | 9         |
| 5.3      | Wave-Expansion-Based Method (WEM) . . . . .                       | 10        |
| 5.3.1    | NFS HFI TFE . . . . .   | 10        |
| 5.3.2    | Weighted Order $\bar{N}$ . . . . .                                | 11        |
| 5.3.3    | Update Process . . . . .  | 11        |
| <b>6</b> | <b>Experiment System</b>  | <b>12</b> |
| 6.1      | General Workflow . . . . .  | 12        |
| 6.2      | Delay-Based Method System . . . . .                               | 13        |
| 6.3      | WEM System . . . . .  | 14        |
| 6.4      | Data Converter and Klippel Automation API . . . . .               | 15        |
| <b>7</b> | <b>Localization of Acoustic Center</b>                            | <b>16</b> |
| 7.1      | List of Research Subjects and Aims . . . . .                      | 16        |
| 7.2      | Simulated Monopole - Fundamental Idea Proposal . . . . .          | 17        |
| 7.3      | Simulated Line Array - Advanced Discussion . . . . .              | 20        |
| 7.3.1    | Delay Method Point Selection . . . . .                            | 21        |
| 7.3.2    | Overfitting and Appropriate Distribution of Coefficient . . . . . | 22        |
| 7.3.3    | Underfitting and Potential Solutions . . . . .                    | 25        |
| 7.4      | JBL Control 1 Pro - Real Measurement . . . . .                    | 26        |
| <b>8</b> | <b>Conclusion</b>   | <b>29</b> |
| <b>A</b> | <b>Method Validity</b>  | <b>31</b> |
| A.1      | Ideal Source . . . . .  | 31        |
| A.2      | Noised Monopole Source . . . . .                                  | 32        |
| <b>B</b> | <b>System Running Processes</b>                                   | <b>33</b> |
| <b>C</b> | <b>JBL Control 1 Pro Brochure</b>                                 | <b>44</b> |

## 1 Company Introduction

Klippel GmbH is a pioneering company in audio system diagnostics and loudspeaker control. Established in 1997 by Prof.Dr. Wolfgang Klippel, the company has dedicated over two decades to product control and measurement methodologies and end-of-line tests for various audio products including loudspeakers, headphones, car audio systems, monitoring devices, and more. With unique measurement devices and completed testing processes, Klippel has become the premier choice providing cutting-edge solutions for audio product improvement and testing to electroacoustic transducer users worldwide.

The company's product fields are primarily divided into R&D solutions for audio product development and Quality Control (QC) software for product testing. The R&D team is responsible for the development of both Klippel software, such as dB Lab, and hardware like Klippel Analyzer 3 (KA3). They also develop numerous modules tailored for transducer measurements, such as the Lumped Parameter Measurement (LPM) module used to acquire Thiele Small parameters of loudspeakers. On the other hand, the QC team provides solutions designed to facilitate fast and comprehensive product testing, ensuring high product quality. The QC software offers a range of powerful features and modules compatible with the KA3. For instance, the Sensitive Rub & Buzz Testing feature detects distortions caused by mechanical defects with high sensitivity. Besides the two main teams, Klippel Controlled Sound Technology (KCS) to let the loudspeaker work as close to the linear range as possible, which can help to build the new generation of the "Green loudspeakers" with less dissipated power.

In addition to offering a comprehensive range of measurement and testing products, Klippel GmbH is dedicated to advancing the education and development of electroacoustic technology. It has established both online and offline courses aimed at providing systematic knowledge learning opportunities for electroacoustic engineers and students alike. Prof.Dr. Wolfgang Klippel presents the highly acclaimed 3-DAY LECTURE "SOUND QUALITY OF AUDIO SYSTEMS", attracting numerous audio professionals seeking to broaden their knowledge base. Furthermore, Klippel's online training provides detailed insights into the measurement principles and solutions of electroacoustic systems, along with comprehensive guidance on the utilization of Klippel systems. This commitment to education and training is a key factor behind Klippel being the preferred choice for many within the audio industry.

## 2 Project Context & Aim

### 2.1 System Under Study - Klippel Near Field Scanner

The radiated sound field and directivity are crucial properties of sound sources such as loudspeakers, musical instruments, and televisions. Traditional methods for measuring directivity typically involve using a turntable and a vertical microphone array to sample spatial points in an anechoic chamber. This approach is time-consuming, costly, and difficult to arrange. To address these challenges and facilitate measurements in normal rooms, Klippel GmbH developed the Near Field Scanner (NFS) and its associated software module in dB-Lab. This system reconstructs and extrapolates the sound field from the near-field holographic measurements. It is based on the principle that an acoustic field can be decomposed into a series of Spherical Waves (SW), which are expressed mathematically with Spherical Harmonic Functions (SHF).

Figure 1a illustrates the Klippel NFS machine. Once the measurement configurations are set, this robotic system moves the microphone along the  $r$ ,  $z$ , and  $\phi$  axes to perform spatial sound field measurements. All raw measurement data and associated metadata are recorded in dB-Lab attachment files as Measurement Data Container (MDC). Figure 1b presents the *Processing* objects used in NFS. In addition to the MDC above, post-processing operations include Holographic Field Identification (HFI) and NFS Visualization. The HFI module identifies sound field characteristics, providing outputs such as total and single SW radiated and apparent sound power spectral curves, fitting configuration details, error curves, and data from a sample measurement point. The NFS Visualization module uses the HFI processing results to extrapolate and represent the sound field in both near-field and far-field regions.

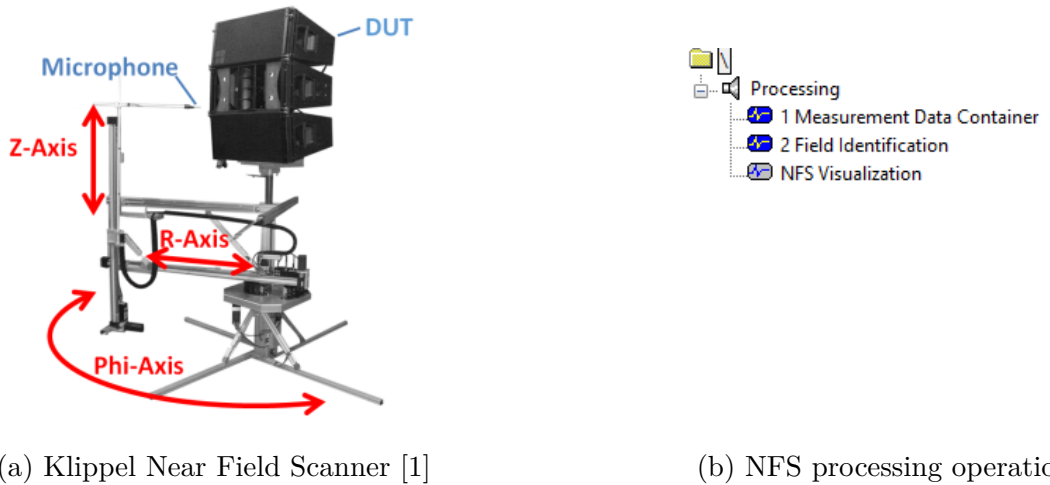


Figure 1: Representation of the Klippel NFS and the related post processing operations.

## 2.2 Necessity of Acoustic Center Localization

During sound field identification with this system, the choice of expansion points can affect the accuracy of the reproduction. However, due to the complexity of the sound field—determined by factors such as driver distribution, crossover networks, materials, mechanical structures, and enclosures—the optimal expansion point varies with frequency and requires expert knowledge to determine. For typical 2-way or 3-way compact loudspeaker systems, the NFS currently uses the tweeter position as the default expansion point. This approach improves identification accuracy at high frequencies and also effectively represents the low-frequency field due to its relatively simple nature. However, this point may not be suitable for other systems, such as line arrays, large multi-way loudspeakers, or distributed mode loudspeakers.

At the same time, correctly localizing the expansion point helps avoid unnecessary compensation with redundant higher-order SW, thereby reducing measurement time. This is because the number of sample points needed for describing the sound field using SW depends on the maximum expansion order. In such cases, accurately locating the correct expansion point—i.e., the acoustic center—is crucial.

Based on this context, the acoustic center is defined as a virtual point from where the SW diverges. Another common definition is as a reference point to which the wave field is traced back, a concept frequently used in far-field sound source localization. This concept can provide a method

to enhance basic fast localization techniques. Additionally, at extremely high frequencies, the sound field becomes too complex to be accurately described using a limited number of SW. In such cases, the second definition of the acoustic center proves to be more effective.

Building on the described research background, this project aims to localize the acoustic center of sound sources, particularly loudspeakers, using two methods: the delay method and the Wave Expansion Based Method (WEM), each corresponding to the two definitions of the acoustic center introduced earlier. The internship involves developing software for acoustic center localization, applicable to both simulated and measured sound fields, and includes visualizing and analyzing experimental results. Additionally, the project outcomes are expected to refine the definition of the acoustic center and reveal its behavior concerning factors such as frequency and sound source characteristics. These advancements are anticipated to benefit related fields in acoustic research, such as virtual acoustics and building acoustics.

### 3 Work Constraint

There are technical constraints during this research. The most crucial and difficult part of the delay method is to measure and calculate the accurate delay time. Although the given algorithms consider the latency in the later sections, it's not always the same for all drivers in a compact active loudspeaker system, which can cause the search failure in some frequency range, like the cross point of the crossover. It's an issue that needs to be clarified and solved.

A technical constraint related to data format compatibility is also identified. While control commands are executed in Python, the database is required to be written in dB-Lab, a platform based on Scilab. During the conversion process between these formats, discrepancies have been observed, particularly affecting data accuracy at higher frequencies. Addressing this issue is crucial to ensure data integrity and should be prioritized in future project phases.

From the WEM's perspective, the primary challenges stem from the lengthy calculation times and the inherent limitations of near-field holographic methods. The current WEM operates by sequentially launching the NFS HFI for each iteration. The duration of each iteration is influenced by factors such as the number of measurement points, the number of frequency points considered, the maximum expansion order, and the number of expansion points. As of the time of writing this report, the development of a parallel processing system has not yet been completed, resulting in WEM optimization processes taking anywhere from 11 minutes to 2 hours, depending on the specific conditions. Given these constraints, the following discussions will not focus on the current time consumption but will instead explore potential ways to reduce the computational time in future implementations.

### 4 Litterature Review

Many researchers have been investigating the localization of the acoustic center for various sound sources across different frequency ranges. Focusing on the low-frequency range, the loudspeaker's directivity is simpler and exhibits fewer lobes, typically expandable in low-order modes such as monopoles and dipoles. John Vanderkooy introduced the concept of the far-field acoustic center in the low-frequency range with two methods [2].

For the first method, unlike the WEM based on SW decomposition, the expression for the multipole expansion is derived from the time-domain Kirchhoff-Helmholtz diffraction equation [3], using the Boundary Element Method (BEM) under the far-field assumption. The theoretical approach involves ignoring the higher-order multipole patterns, particularly the dipole pattern. When observed from this acoustic center, the loudspeaker's directivity appears nearly uniform in all directions. Thus, the acoustic center can be approximated as the center of the radiating monopole.

The mathematical derivation from this research provides a theoretical guideline for determining the location of the precise acoustic center position of a point source on a baffle. It suggests that the acoustic center is approximately located at a distance of  $2/3$  times the radius of the baffle in front of the point source, and after a certain boundary frequency the center becomes closer to the membrane.

This conclusion is supported through the second method employing the  $1/r$  response in low-frequency measurements with a sealed box loudspeaker. This method is based on the monopole propagation formula  $p(r) \propto e^{-jkr}/r$ . The phenomenon is illustrated in Figure 2. The position offset of the acoustic center from the origin, denoted by  $\Delta$ , is determined by measuring the pressure field at points both in front and behind the loudspeaker.

M.D. Cola et al. validated this effect using three distinct measurement methods involving subwoofer sources, one of which is based on holographic directivity measurements with Klippel NFS—the primary experiment tool employed in this research [4]. Building on the same theoretical foundation, the concept of the acoustic center has been extended to other common source models. Samuel D. Bellow provides explicit derivations and discussions regarding the acoustic center configurations for both spherical and non-spherical sources at low frequencies [5].

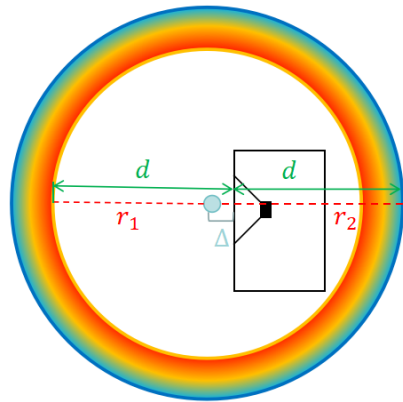


Figure 2:  $1/r$  Response method clarification.

In addition to previous discussions on monopole acoustic centers, there are studies focused on acoustic centers derived from SW expansion. Samuel D. Bellows et al. localized the acoustic center of musical instruments using wave expansion [6]. Their approach, which also focuses on the far-field, is based on the theory that wave propagation follows an inverse proportional relationship with distance  $r$  in the infinity far field [7]. The method involves using an optimization algorithm to identify the acoustic center such that the fields characterized by  $1/r$  propagation and SW decomposition are aligned.

However, the optimized far-field wave expansion method requires conventional directional measurements, which are done in anechoic chambers with constructed microphone arrays. As mentioned before, the measurements are time-consuming and money consuming. Moreover, this method encounters challenges such as spatial sampling resolution and room effects in the far-field. Although time windows can remove room reflections, their effectiveness is limited to low frequency ranges [8].

To address these limitations, the Klippel NFS offers an advanced solution for sound field measurement and reproduction. W. Klippel et al. have detailed the operational principles of the Klippel NFS in their work [8] [1], which is essential for understanding the fundamental concepts of this project. As previously mentioned, the Klippel NFS utilizes spherical wave expansion. The measured transfer functions of the sound sources,  $H(f, \mathbf{r}_i) = P(f, \mathbf{r}_i)/U(f)$ , are expanded to extrapolate the sound field.

Equation (1) presents the theoretical solutions of the wave propagation equation in spherical coordinates. The detailed derivations are given by Earl G. Williams [7]. This equation can be expanded and rewritten in the form of vector multiplication, as described in [1].

$$H(f, \mathbf{r}_i) = \sum_{n=0}^{N(f)} \sum_{m=-n}^n C_n^m(f) h_n^{(2)}(kR_i) Y_n^m(\theta_i, \phi_i) = \mathbf{C}(f)^T \mathbf{b}(f, \mathbf{r}_i). \quad (1)$$

It should note that  $Y_n^m(\theta_i, \phi_i)$  represents the spherical harmonic functions, with their real parts illustrated in Figure 3. The vector  $\mathbf{r}_i = (R_i, \theta_i, \phi_i)$  denotes the coordinate vector of the observation point relative to the expansion point  $\mathbf{r}_E$ , where  $\theta$  and  $\phi$  represent the elevation and azimuth angles, respectively. The coefficient vector is represented by  $\mathbf{C}(f)$ , while  $\mathbf{b}(f)$  represents the remaining components. The harmonics of different orders are weighted by the outgoing Hankel functions  $h_n^{(2)}$  and coefficients  $C_n^m(f)$ , which varies with frequency.  $G$  represents the set of measurement points on the grid.

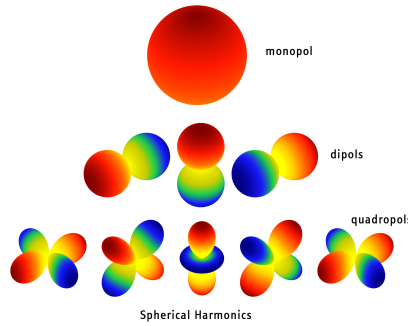


Figure 3: Directivity balloon of the real parts of the Spherical Harmonic Functions [9].

Given the input expansion conditions, such as the acoustic center and the frequency set, the values of both the Hankel functions and the SHF are known at any given point. The critical task is to determine the corresponding weighted coefficients  $C_n^m(f)$ . The Klippel NFS optimizes these coefficients  $\hat{C}_n^m(f)$  by minimizing the deviation between the measured sound field and the fitted sound field, as described in Equation (2) and Equation (3).

$$\hat{C}_n^m(f) = \operatorname{argmin}_{C(f)} \left( \sum_{\mathbf{r}_{m,i} \in G} |e(f, \mathbf{r}_i)|^2 \right), \quad (2)$$

$$e(f, \mathbf{r}_i) = H(f, \mathbf{r}_i) - \sum_{n=0}^{N(f)} \sum_{m=-n}^n \hat{C}_n^m(f) h_n^{(2)}(kR_i) Y_n^m(\theta_i, \phi_i). \quad (3)$$

The optimal parameter values are obtained through the matrix Equation (4), where  $\mathbf{H}_m(f)$  is the vector of measured transfer functions across all points, and  $\mathbf{B}(f, \mathbf{r}_E)$  represents the set vector corresponding to  $\mathbf{b}(f, \mathbf{r}_i)$ . The final expression uses the variable  $\mathbf{r}_E$  instead of  $\mathbf{r}_i$  because it encompasses all measurement points.

$$\hat{\mathbf{C}}(f, \mathbf{r}_E) = \mathbf{H}_m(f) \mathbf{B}(f, \mathbf{r}_E) \left( \mathbf{B}(f, \mathbf{r}_E) \mathbf{B}(f, \mathbf{r}_E)^T \right)^{-1}. \quad (4)$$

With the given start point, the measurement array calculated by the NFS is a projection of the optimized points corresponding to the SW lobe distributions from a sphere onto two different cylindrical layers, aided by random auxiliary points. This setup not only ensures accurate fitting of the sampled sound field but also considers wave propagation modeling. Consequently, it allows for valid extrapolation in both near-field and far-field conditions, thereby enhancing the efficiency and reliability of the measurement data. This also highlights the importance of choosing the correct expansion point.

## 5 Theory Framework

This project is developed based on two methods: the delay method and the WEM. The delay method considers the fundamental nature of sound propagation, where sound waves travel according to the speed formula  $t_d = \frac{R}{c}$  in a uniform medium without boundaries. In this formula,  $t_d$  denotes the delay time,  $R$  denotes the distance between the sound source and the measurement point, and  $c$  is the speed of sound in the current environment. The specific process of acoustic center localization is implemented using the Least Mean Square (LMS) algorithm and the Difference of Arrival Linearization Matrix (DALM) algorithm, respectively, to find the point where the measurement delay time equals the sound traveling time.

The delay method requires highly accurate delay time measurements. The robust effects, like the background noise and the uncertain latency of the active drivers, can completely confuse the localization result. In contrast, the WEM is more compatible with the Klippel NFS and less affected by the latencies. It employs adaptive algorithms to update the expansion points, thereby identifying the acoustic center that minimizes the fitting error or the weighted order  $\bar{N}$ . In this project, the acoustic center is localized and analyzed by both methods.

### 5.1 Simulated Sound Field

For the simulation cases, the sound fields received at the measurement points are determined by the configuration of the sound sources. This section describes the selected simulated source models and the method used to calculate the frequency response.

Reasonable and simple simulated sound sources are valuable for validating the method and demonstrating the ideal outcomes of acoustic center localization. The primary sound sources studied in this project are loudspeakers. Various models for loudspeaker radiation sound fields have been developed, such as the Distributed Edge Dipole model [10]. Most of these models are based on BEM principles,

representing loudspeakers as a combination of monopoles and dipoles. A dipole can be also considered as a pair of monopoles close together with opposite amplitudes in the far field. Therefore, this research only focuses on the monopole unit and white noise, which is used for noise simulation.

Combining the multipole model with SW theory yields the radiated pressure and power, as shown in Equation (5) and Equation (6), where  $P_{\text{mono}}$  is the radiated power in dB. Given a constant  $\Pi_{\text{mono}}$ , the monopole sound field is as Equation (7).

$$\hat{p}_{\text{mono}}(f) = C_{00} \frac{e^{-ikR_i}}{R_i}. \quad (5)$$

$$\Pi_{\text{mono}} = \frac{1}{2\rho_0 c k^2} |C_{00}|^2, \quad P_{\text{mono}} = 10 \log_{10} \left( \frac{\Pi_{\text{mono}}}{\Pi_{\text{ref}}} \right). \quad (6)$$

$$\hat{p}_{\text{mono}}(f) = \sqrt{\left( \Pi_{\text{ref}} 10^{\frac{P_{\text{mono}}}{10}} 2\rho_0 c k^2 \right)} \frac{e^{-ikR_i}}{R_i}. \quad (7)$$

In the equation,  $P_{\text{ref}}$ ,  $\rho$  and  $c$  are the reference sound power, air density, and the sound speed in the air,  $k = \frac{2\pi f}{c}$  is the wave number and  $R_i$  is the relative distance between the monopole and the observation point. According to this equation, the pressure  $i$ -th measurement point, generated by a sum of monopoles, is given by  $\hat{p}_i(f) = \sum_j \hat{p}_{\text{mono},j}(f)$ . White noise is treated as a point source with a constant amplitude determined by the signal-to-noise ratio (SNR), and its phase follows a normal distribution. Their amplitude is  $P_{\text{white noise}} = \frac{P_{\text{mono}}}{\log_{10}(\text{SNR})}$ .

## 5.2 Delay Method

The method is based on Cartesian coordinates and initially assumes that the system latency is constant. It involves four unknown variables: the coordinates of the acoustic center  $\vec{r}_o = (x_o, y_o, z_o)$  and the latency  $\tau_0$ . The delay method utilizes measurement data from points in the sound field, as illustrated in Figure 4. The position of the  $i$ -th measurement point  $\vec{r}_i = (x_i, y_i, z_i)$  is known and the corresponding delay time  $t_{m,i}$  can be measured. The correct acoustic center solution ensures that each measurement point satisfies the speed formula mentioned earlier, in addition to accounting for latency. The expanded error equation with the specified coordinates is represented in Equation (8). This section introduces the theoretical details of the LMS algorithm and DALM algorithm.

$$e_i = t_{m,i} - \tau_0 - \frac{|\vec{r}_i - \vec{r}_o|}{c} = t_{m,i} - \tau_0 - \frac{\sqrt{(x_i - x_o)^2 + (y_i - y_o)^2 + (z_i - z_o)^2}}{c}. \quad (8)$$

### 5.2.1 Group Delay

The measured delay time used in this method is the mean group delay. Group delay is a frequency-domain property of the signal that describes the time shift of the envelope at a particular frequency. The group delay  $t_{m,i}(f)$  is expressed as Equation (9), where  $\phi(f)$  represents the phase response of the transfer function  $H(f)$ .

$$t_{m,i}(f) = -\frac{1}{2\pi} \frac{\partial \phi(f)}{\partial f}. \quad (9)$$

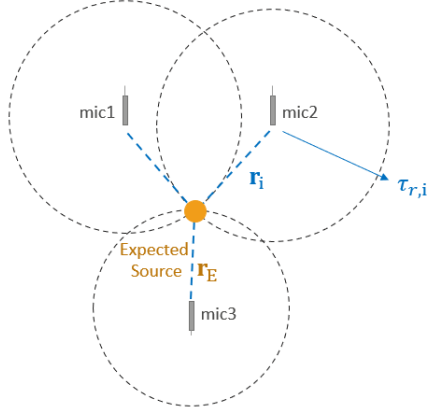


Figure 4: Representation of the theoretical principles of the delay method.

In an ideal linear system, the group delay should remain constant. However, in practical applications, issues such as noise, room reflections, and environmental variations like temperature change distortions. The group delay response can be used to calculate the average delay time over a frequency range, thereby decreasing the influence of these factors. Additionally, since the acoustic center is frequency-dependent, the group delay response is useful for localization across different frequency ranges.

### 5.2.2 LMS Algorithm

The basic idea of the LMS algorithm is to find the derivative of the error equation concerning the target parameters and use this as a step to update the system parameters. For example, the update equation for the expected coordinate  $x_E$  is given by  $x_E(k+1) = x_E(k) - \mu_x \frac{\partial e(x_E)}{\partial x_E}$ . With  $N$  measurement points and their data, the localization error for an arbitrary expected point as the acoustic center is shown in Equation (10).

$$e_E = \sum_{i=1}^G \left( t_{m,i} - \tau_0 - \frac{|\vec{r}_i - \vec{r}_E|}{c} \right) = \sum_{i=1}^G \left( t_{m,i} - \tau_0 - \frac{\sqrt{(x_i - x_E)^2 + (y_i - y_E)^2 + (z_i - z_E)^2}}{c} \right). \quad (10)$$

Unlike the common application of the linear LMS algorithm, this error equation introduces a multi-variable nonlinear problem. However, since the length of each variable is one and calculating the derivative of the error equation is not challenging, the algorithm can be applied effectively. The three coordinates  $x_E$ ,  $y_E$  and  $z_E$  follow the same form, the general updating equation for the three coordinates is represented in Equation (11), with  $q = x, y, z$  and  $R_{iE}(k) = \sqrt{(x_i - x_E(k))^2 + (y_i - y_E(k))^2 + (z_i - z_E(k))^2}$ .

$$q_E(k+1) = q_E(k) - \mu_q \frac{\partial e(q_E)}{\partial q_E} = q_E(k) - \mu_q \sum_{i=1}^G \frac{2}{c^2} (q_i - q_E) \left( \frac{(t_{m,i} - \tau_0(k)) \cdot c}{R_{iE}(k)} - 1 \right). \quad (11)$$

The updating equation of the latency  $\tau_0$  is linear and expressed as the Equation (12).

$$\tau_0(k+1) = \tau_0(k) - \mu_\tau \frac{\partial e(\tau_0)}{\partial \tau_0} = \tau_0(k) - \mu_\tau \sum_{i=1}^G \frac{R_{iE}(k)}{c} \left( \frac{(t_{m,i} - \tau_0(k)) \cdot c}{R_{iE}(k)} - 1 \right). \quad (12)$$

It can be observed that there is a common factor for both the coordinate variables and the latency, which can be expressed in a simplified form as  $b_i(k) = \left( \frac{(t_{m,i} - \tau_0(k)) \cdot c}{R_{iE}(k)} - 1 \right)$ . The four adaptive variables are updated simultaneously in practical applications. Otherwise, the variables cannot converge to the minimum error achievable by setting the step factor to  $\mu_q$  due to the mutual restriction between the variables. Each update equation can be represented as shown in Equation (13),

$$\vec{q}(k+1) = \vec{q}(k) - \vec{\mu} \cdot (M(k) \times \vec{b}(k)), \quad (13)$$

where

$$\vec{q}(k) = (x_E(k), y_E(k), z_E(k), \tau_0(k))^T; \quad \vec{\mu}(k) = (\mu_x, \mu_y, \mu_z, \mu_\tau)^T;$$

and

$$M(k) = \begin{pmatrix} \frac{2(x_1 - x_E(k))}{c^2} & \dots & \frac{2(x_i - x_E(k))}{c^2} & \dots & \frac{2(x_G - x_E(k))}{c^2} \\ \frac{2(y_1 - y_E(k))}{c^2} & \dots & \frac{2(y_i - y_E(k))}{c^2} & \dots & \frac{2(y_G - y_E(k))}{c^2} \\ \frac{2(z_1 - z_E(k))}{c^2} & \dots & \frac{2(z_i - z_E(k))}{c^2} & \dots & \frac{2(z_G - z_E(k))}{c^2} \\ \frac{R_{1E}(k)}{c} & \dots & \frac{R_{iE}(k)}{c} & \dots & \frac{R_{GE}(k)}{c} \end{pmatrix}_{4 \times G}; \quad \vec{b}(k) = \begin{pmatrix} b_1(k) \\ \vdots \\ b_i(k) \\ \vdots \\ b_G(k) \end{pmatrix}_{G \times 1}.$$

### 5.2.3 DALM Algorithm

Due to its multi-variable and nonlinear properties, this issue does not have a corresponding Wiener filter solution [11], unlike common adaptive problems. Instead, linearized matrix equations, such as the Wiener-Hopf equation, are suitable for this problem and can quickly locate the solution. This can be achieved and solved directly by performing the subtraction operation to obtain the DALM matrix.

The derivation begins by eliminating the square root sign of the Equation (8) and applying the quadratic equation. The expanded equations for the  $i$ -th and  $j$ -th measurements are shown below :

$$(x_o^2 + x_i^2 - 2x_o x_i) + (y_o^2 + y_i^2 - 2y_o y_i) + (z_o^2 + z_i^2 - 2z_o z_i) = (\tau_0^2 + t_{m,i}^2 - 2\tau_0 t_{m,i})c^2 \quad (14)$$

$$(x_o^2 + x_j^2 - 2x_o x_j) + (y_o^2 + y_j^2 - 2y_o y_j) + (z_o^2 + z_j^2 - 2z_o z_j) = (\tau_0^2 + t_{m,j}^2 - 2\tau_0 t_{m,j})c^2.$$

The subtraction of the above two equations can eliminate all unknown squared terms, resulting in a linear equation as shown in Equation (15), where  $C_{ji} = \Delta x_{ji}^2 + \Delta y_{ji}^2 + \Delta z_{ji}^2 - \Delta t_{m,ji}^2 c^2$ . Here,  $\Delta$  denotes the difference, such that  $\Delta x_{ji} = x_i - x_j$  and  $\Delta x_{ji}^2 = x_i^2 - x_j^2$ .

$$2(\Delta x_{ji} \ \Delta y_{ji} \ \Delta z_{ji} \ \Delta t_{m,ji} c^2) \begin{pmatrix} x_o \\ y_o \\ z_o \\ \tau_0 \end{pmatrix} = C_{ji}. \quad (15)$$

According to the above equation, the results can be obtained using only four pairs of points. To reduce the influence of noise and avoid singular matrices, an optimized solution is computed by solving an overdetermined system with more pairs of points. The approximate solutions are obtained using QR factorization [12]. With  $G$  measurement points, there are a total  $\frac{G(G+1)}{2}$  combinations possible. These combinations can be used to construct a matrix equation:

$$\mathbf{A}\mathbf{q} = \mathbf{v}, \quad (16)$$

where it can be expanded as the Equation

$$\begin{pmatrix} \Delta x_{21} & \Delta y_{21} & \Delta z_{21} & \Delta t_{m,21}c^2 \\ \vdots & \vdots & \vdots & \vdots \\ \Delta x_{G(G-1)} & \Delta y_{G(G-1)} & \Delta z_{G(G-1)} & \Delta t_{m,G(G-1)}c^2 \end{pmatrix}_{\frac{G(G-1)}{2} \times 4} \begin{pmatrix} x_o \\ y_o \\ z_o \\ \tau_0 \end{pmatrix}_{4 \times 1} = \begin{pmatrix} C_{21} \\ \vdots \\ C_{G(G-1)} \end{pmatrix}_{\frac{G(G-1)}{2} \times 1}. \quad (17)$$

### 5.3 Wave-Expansion-Based Method (WEM)

This method localizes the acoustic center by adjusting the expansion points to minimize the Total Fitting Error (TFE) or the weighted order  $\bar{N}$ . The TFE directly reflects the quality of fit for the reconstructed radiated sound field [1]. Under ideal conditions, TFE serves as a reasonable criterion for finding the acoustic center. However, due to the complexity of SW and the influence of robust factors, such as the background noise, the efficiency and accuracy of localization using TFE significantly depend on the chosen expansion order.

To address this, the concept of the weighted order  $\bar{N}$  is introduced. Similar to the center of gravity, the weighted order represents the central order of radiated power. This parameter provides insights into the distribution of radiated power across different orders and helps determine the optimal expansion order. Moreover, by updating the expansion point to achieve a lower  $\bar{N}$  value, the fitting process becomes more efficient. Since the number of measurement points  $M_m$  is related to the maximum expansion order, as shown in Equation (18), a lower  $\bar{N}$  reduces the required expansion order. The theories of TFE and  $\bar{N}$  are discussed in detail in the following subsections.

$$M_m \geq (N_{\max} + 1)^2 \quad (18)$$

#### 5.3.1 NFS HFI TFE

The TFE, as mentioned earlier, is calculated in the Klippel NFS HFI module, with its equation given below:

$$\text{TFE} = 10 \log \left( \frac{\sum_{\mathbf{r}_i \in G} |e(f, \mathbf{r}_i)|^2}{\sum_{\mathbf{r}_i \in G} |H(f, \mathbf{r}_i)|^2} \right), \quad (19)$$

where  $e(f, \mathbf{r}_i)$  is the same variable as in Equation (3) and  $H(f, \mathbf{r}_i)$  is the transfer function. Figure 5 provides an example of the Klippel NFS HFI TFE chart.

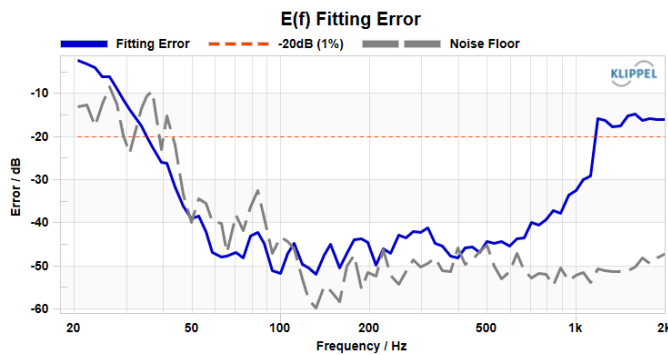


Figure 5: Example of a Klippel NFS HFI TFE chart, including both the TFE curve and the noise floor curve.

The TFE is a highly constrained parameter that assesses not only the amplitude fitting of the expanded waves but also their phase. Additionally, as mentioned previously, with measurements taken at two layers of points, the sound field's propagation processes are considered, which can reduce the specificity of the fitted coefficients. Consequently, a low TFE indicates a reliable reproduction of the sound field. For standard evaluation, a threshold of -20 dB is set as a benchmark for good fitting, signifying at least a 99% fit.

### 5.3.2 Weighted Order $\bar{N}$

The choice of expansion order significantly influences the fitting accuracy in acoustic center localization—whether it results in underfitting, good fitting, or overfitting—issues that are central to the discussions in Section 7. In this project,  $\bar{N}$  is also regarded as an update standard for WEM same as TFE to optimize and discuss.

As illustrated earlier, the weighted order  $\bar{N}$  is a concept related to the radiated power. The radiated power's formula of the  $n$ -th SHF is given by Equation 20 [7], where  $\vec{v}_{r_n}^*$  represents the conjugation of the radial velocity determined by the Euler equation,  $r$  is the observation radius, and  $d\Omega$  is the differential solid angle. In the NFS, the radiated transfer function  $H(f)$  is used to calculate the power instead of pressure, which eliminates the influence of the input voltage signal.

$$\Pi_n(f) = \int I_{r_n}(f) r^2 d\Omega = \frac{1}{2} \int \operatorname{Re} \left( p_n(f) \vec{v}_{r_n}^*(f) \right) r^2 d\Omega \quad (20)$$

Similar to the expressions of the fitted transfer functions  $H(f)$ , the total radiated power spectrum and that of each SHF can be directly represented using the optimized coefficient values  $\hat{C}_n^m(f)$  obtained through NFS HFI. Figure 6 shows an example result of the field identification at  $f = 1\text{kHz}$  and the maximum expansion order is  $N(f) = 10$ . Using the radiated power distribution calculated by NFS HFI, the weighted order  $\bar{N}(f, \vec{r}_{exp})$  is obtained by Equation (21).

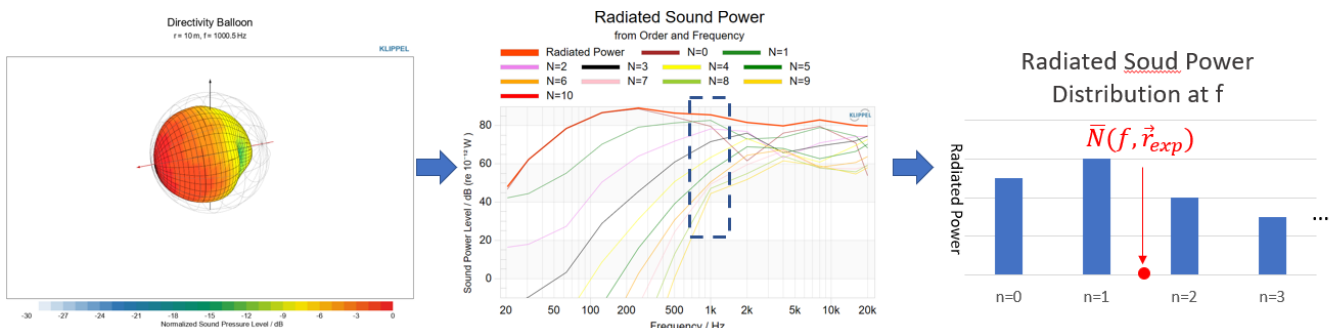


Figure 6: Example of the radiated sound power distribution and the concept of the weighted order.

$$\bar{N}(f, \vec{r}_{exp}) = \frac{\sum_{n=0}^{N(f)} n \Pi_n(f, \vec{r}_{exp})}{\sum_{n=0}^{N(f)} \Pi_n(f, \vec{r}_{exp})}. \quad (21)$$

### 5.3.3 Update Process

The update process of the WEM is detailed in Diagram 7. Instead of shifting by a single specified vector, a new expansion point cloud is generated using an update step  $h$ . By default, the point cloud includes 8 corner points and 6 face center points of a cube with a side length of  $2h$ , centered on

the current expansion point. The TFE and  $\bar{N}$  values of all points in the cloud are calculated and compared. If the minimum value corresponds to a new point, that point becomes the next expansion point. If the current point retains the minimum value, the update step  $h$  becomes the half value  $h/2$ . The process continues until a specified number of iterations is reached, which serves as the stopping criterion.

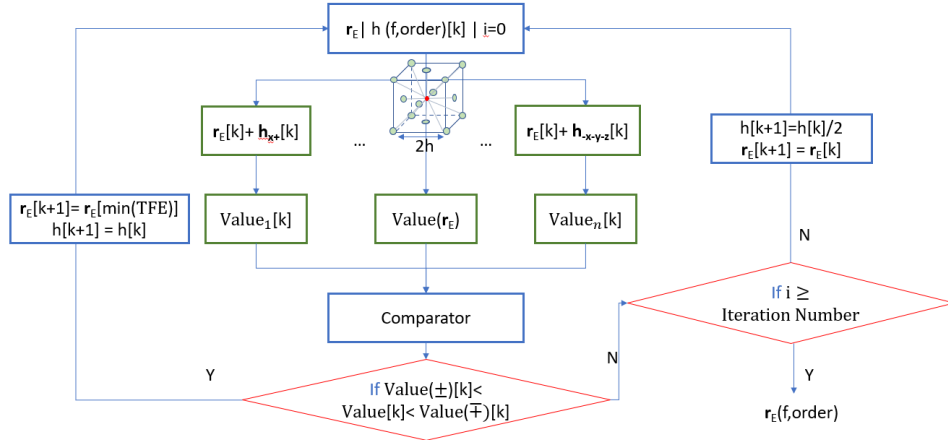


Figure 7: Schematic diagram of updated principle of the WEM.

## 6 Experiment System

### 6.1 General Workflow

The experiments for acoustic center localization are conducted for both simulated and real sound sources. Figure 8 shows the general workflow of the experimental system, where the green boxes represent data or commands in Python format, and the orange boxes represent those in dB-Lab. Other colors are used for distinction purposes only. As shown in the workflow diagram, the algorithm implementation and signal processing for delay-based methods are completed in Python. For the WEM, the processing command is in Python, and the implementation is primarily done in the Klippel NFS NFI module, which is in dB-Lab.

The acoustic center of both simulated and real sound sources needs to be localized using two methods. Therefore, it is necessary to prepare data containers in both Python and dB-Lab for processing. The raw data for simulated sound sources is managed in Python, while the measured data for real sources is stored in the NFS MDC format in dB-Lab. A data converter has been implemented in the system using the Klippel Automation (KlAutomation) Application Programming Interface (API) to enable the transformation between these two types of raw data. Section 6.4 provides a brief overview of how the KlAutomation API is utilized. It is important to note that the raw data for each measurement point includes its coordinate values, latency, impulse response, and the corresponding time axis.

The workflow also highlights the use of additional .txt files. Given the large volume of processing data and the complexity of the data types, key parameters are recorded in .txt files and then re-imported into Python for visualization. Additionally, it is recommended to use a new dB-Lab file as a container for storing the post-processing data of the WEM. Appendix B provides detailed information

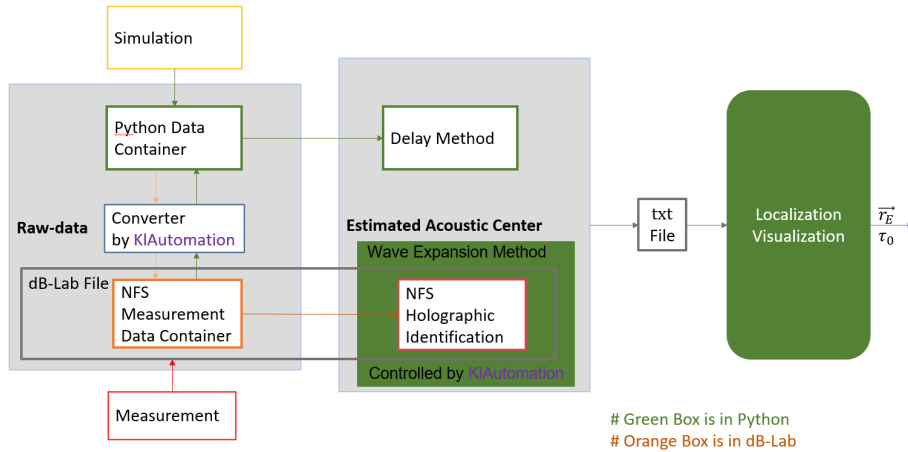


Figure 8: Schematic diagram of the overall workflow of the experimental system software processing.

on the code structure of the experimental and visualization systems, the data format for recorded .txt files, and examples of the Python interface.

The following sections provide detailed descriptions of the developed experimental system from the perspective of the two methods: Section 6.2 covers the delay method, and Section 6.3 focuses on the WEM.

## 6.2 Delay-Based Method System

Figure 9 illustrates the implementation process of the delay method, from setting up the raw-data container to applying the algorithms. The key input data for the delay method includes the coordinates and measured delay times, which are detected and calculated from the Impulse Response (IR) at the specified measurement points.

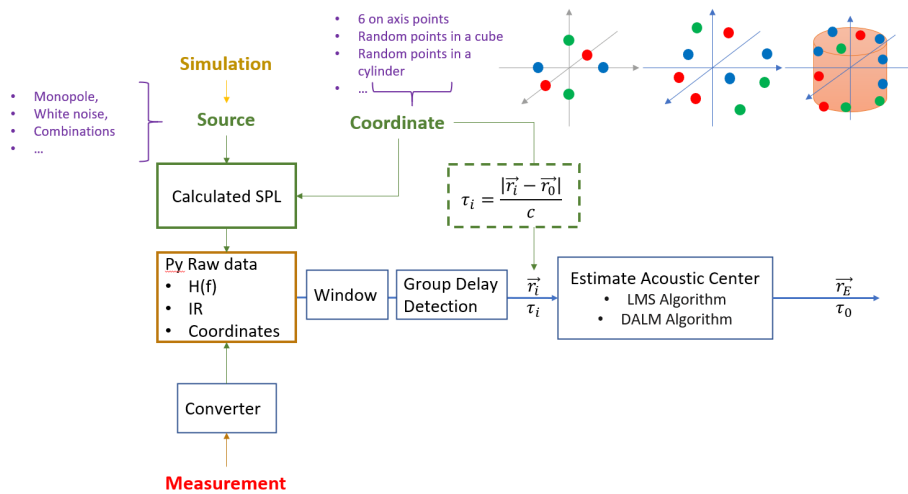


Figure 9: Schematic diagram of the delay-based method of the experimental system software processing.

For measurements, the raw data is extracted and converted from the NFS MDC. For simulations, the raw data container is created based on user-defined sound sources and measurement points. As

mentioned before, the available sound source options include monopole and white noise, allowing simulation of both simple and complex sound fields through various combinations and parameter settings. The calculation theories are clarified in Section 5.1. And the simulated set of measurement points is provided in three different sets: six on-axis points at a specified distance, a set of random points within a cubic boundary, and a set of random points on a cylinder with known dimensions.

However, the IR cannot be directly used to detect the group delay, especially in measurement cases due to room reflections. To address this, the IR is first windowed using a Tukey window with  $r=0.5$ . The length of the window is set to the shortest distance free of reflections, determined by the relative positions of the sources and the room setup. Applying a window is a conventional and effective method for mitigating high-frequency room effects. However, low-frequency reflection issues remain unaddressed. The advanced Klippel in-situ measurement algorithm has not been integrated into this project. Consequently, for the current measurement setup, the delay method is only effective at high frequencies.

There are two ways to calculate the delay time (without latency), each serving a different purpose. The straightforward method uses the distance divided by the sound speed to obtain the delay time value. This method only validates the algorithms for ideal simulated sound sources. In real localization problems, the delay time is the averaged group delay response over the focused octave frequency range. Due to time constraints, experiments accounting for latencies were not conducted.

The fundamental validation of the delay method's effectiveness across various algorithms is detailed in Appendix A. In the final experimental system, the delay method begins with the DALM algorithm to establish an initial starting point. Subsequently, the LMS algorithm refines these results by using the DALM outputs as starting points. The outcomes of both algorithms are presented and discussed in the following sections. Further explanation is omitted here.

### 6.3 WEM System

The WEM aims to optimize the expansion point to obtain the minimum  $\bar{N}$  value. The method workflow represents the approximate process as shown in Figure 10. The initial fitting error can be calculated in the HFI module using the measured NFS data container or the one converted from the simulated Python data container, and the initial field identification setup, including the expansion point position and the maximum expansion order. Then, the algorithm updates the expansion point position and performs a new field identification. This update process can be automated according to theory of Section 5.3.3 combining with KlAutomation API.

Figure 11 displays the optimization running record of the WEM in dB-Lab. For each frequency, the data from each iteration is stored in an object, with its name indicating the processing frequency, iteration index, and center coordinates. The expanded points from the previous center are labeled according to their HFI operation. Figure 11a shows an example of these recorded processes. Upon completing an iteration, the data for the next center is stored in a history object for that frequency. When the localization process runs across multiple frequencies, the center history data is aggregated as shown in Figure 11b.

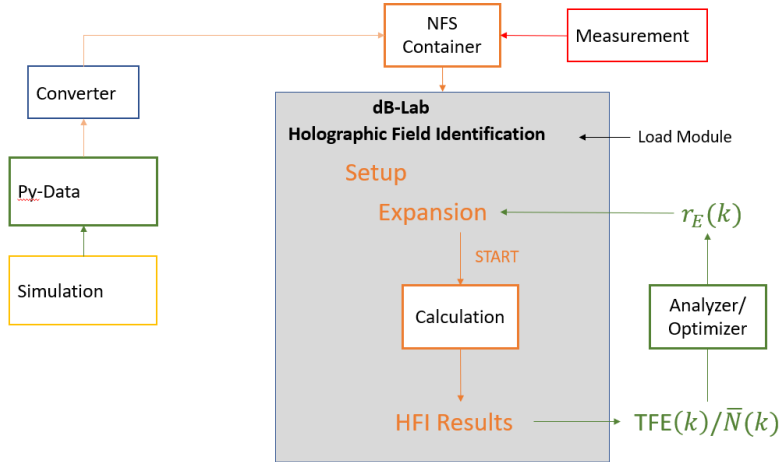


Figure 10: Schematic diagram of the wave-expansion-based method of the experimental system software processing.

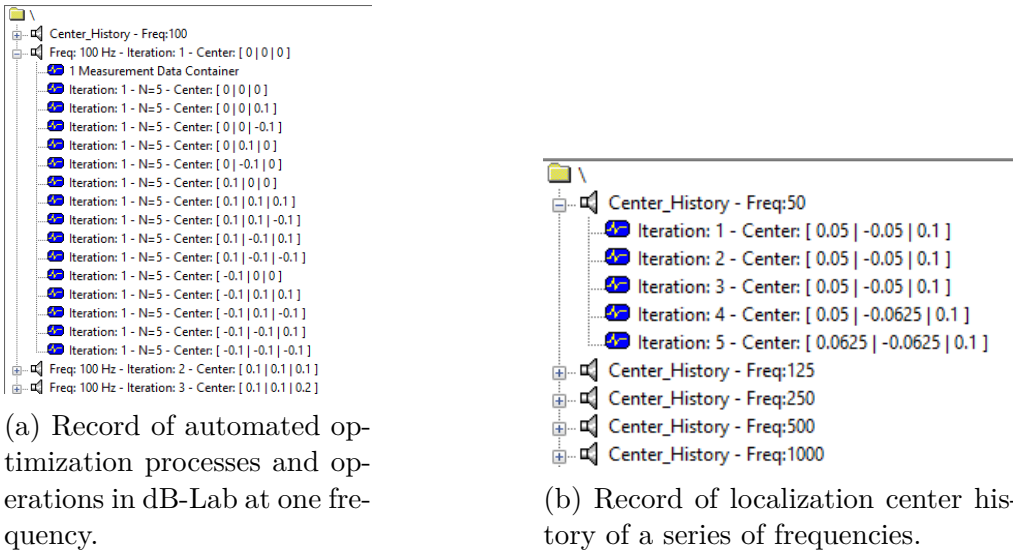


Figure 11: Running record of the WEM optimization processes.

## 6.4 Data Converter and Klippel Automation API

One of the most crucial components in the system is the data converter, which enables the conversion between Python data and Scilab data for integration into the NFS MDC operation within dB-Lab. The converted data is stored in dB-Lab as **Attachments**—a series of individual "files" that contain the data and are named to reflect their content. The term "files" is in quotes because these are not actual files but variables within the **Attachments node**. dB-Lab is organized using a node-based structure, where drivers, operations, and each subfunction are represented as nodes within a larger, circuit-like framework. The recording, reading, and modification of data under each node can be performed via the Klippel Automation API.

Klippel provides the KIAutomation API, which can be implemented in various programming languages, such as Python and C#. This API allows software components to be created as COM/ActiveX objects within an application [13]. KIAutomation enables remote operations without the need to manually open dB-Lab, including accessing node attachments, recording information, and modify-

ing data. The general process for converting Python data to NFS MDC involves first reorganizing the calculated data to match the NFS MDC structure, then using KlAutomation to open dB-Lab, record the data information, and set the values. The inverse process is similar: first, data values are retrieved and classified by identifying their associated information using KlAutomation, and then the data is reorganized to fit the DataContainer() class for use in Python.

It should be noted that the data transformed from NFS MDC to Python represents raw, untreated data. Post-processing steps to remove background noise and room effects, such as signal windowing and ingoing wave identification, have not yet been applied.

## 7 Localization of Acoustic Center

This section presents and analyzes the acoustic center localization results for different simulated or actual measurement scenarios. Since acoustic center is a multi-interpreted concept and the actual sound field is complex, this study does not provide a precise definition of the acoustic center in the context of the Klippel NFS, but rather explores the application of the methods discussed in this report from different perspectives depending on the specific objectives.

### 7.1 List of Research Subjects and Aims

Figure 12 outlines the research subjects and aims of this report. The study examines three primary subjects: a simulated monopole, a simulated line array composed of two monopoles with opposite amplitudes, and a real-world measurement involving the passive 3-way loudspeaker JBL Control 1 Pro. The experimental scenarios progress from simple to more complex setups. All three subjects are analyzed using three localization processes, which apply the delay method and the WEM according to both the TFE and  $\bar{N}$  standards.

The results of the simulated monopole at a single frequency are presented and analyzed to establish a general understanding of the localization processes. For the other two examples, the results are demonstrated across multiple frequencies.

The localization results are presented and analyzed based on a series of objectives. One of the primary aims is to fit the sound field better and reproduce it with greater accuracy, which is directly reflected in achieving a lower TFE. Another key objective is to enhance the efficiency of the fitting process, which involves minimizing the number of measurement points and utilizing a lower-order representation of the sound field.

Additionally, the results provide valuable insights for two research goals. First, the study aims to determine the appropriate order distribution of SHFs to enhance the extrapolation of the reconstructed sound field using the Klippel NFS in both the Near-Field and Far-Field. It is important to note that the appropriate order distribution does not always have the lowest TFE value, but rather a good fit that is not order-compensated and well describes the propagation of the waves radiated by the source itself. Second, inspired by the works of Vanderkooy, the study further researches the specific acoustic center concept by employing a lower-order representation of the sound field. This approach can reduce resolution dependency and significantly improve the accuracy of back lobes.

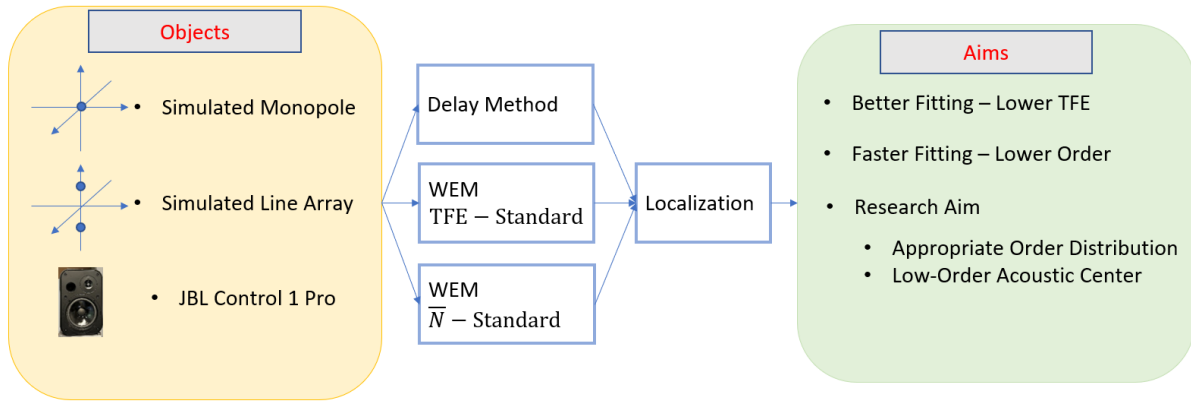


Figure 12: Schematic diagram of the workflow for the implementation of the acoustic center localization experiment for different sound sources.

## 7.2 Simulated Monopole - Fundamental Idea Proposal

The simplest sound field is that of a monopole, which propagates omnidirectionally in a steady state across all frequencies. In a free field, the delay time of the sound produced by a monopole conforms to the speed equation. Additionally, the low-frequency behavior of common compact loudspeaker systems can be approximated as monopole-like due to the long wavelength involved. Therefore, the simulated monopole serves as an effective model for research.

Figure 13 illustrates the details of the experimental setup, including the coordinates of the sound source, the number of measurement points, and their geometric distribution. No delay was introduced in this setup. The three localization methods used include a hybrid algorithm in the delay method: first, the DALM matrix method for initial detection, followed by the LMS algorithm for precise optimization. Additionally, the WEM with the TFE standard and the weighted order  $\bar{N}$  standard are employed. The tables on the right display the initial setup parameters and expansion conditions for the processes. This configuration table is essential for all simulation and measurement cases, aiding in the comparison of localization results with the expected center position and in analyzing the sources of errors. In this case, the observation frequency is 100 Hz, and the maximum expansion order is 5.

| Parameters           | Setup Value   |
|----------------------|---|
| Source Type          | Ideal Monopole  |
| Source Position      | (0.052,0.1,0.246)   |
| Localization Method  | Delay Method : TDoA+LMS<br>WEM : TFE<br>WEM: Weighted Order |
| Initial Point        | (0,0,0)   |
| Frequency            | 100Hz   |
| Point Number         | 500   |
| Measurement Cylinder | Cylinder 1 : (r=0.5,h=0.8)<br>Cylinder 2 : (r=0.6,h=0.9)    |

| Delay Method            |                       |
|-------------------------|-----------------------|
| WEA Iteration           | 1000                  |
| steps                   | (1,1,1)               |
| Method                  | First TDOfA, then LMS |
| WEA Method              |                       |
| Iteration               | 10                    |
| Initial Steps           | 0,1                   |
| Maximum Order           | 5                     |
| Point Number per Octave | 1                     |

Figure 13: Experiment configuration of the simulated monopole.

Figure 14 shows the update curves for the three coordinate positions. The DALM method successfully localizes the correct positions in one step, and the LMS algorithm maintains these positions accurately. This result is expected for the ideal monopole model.

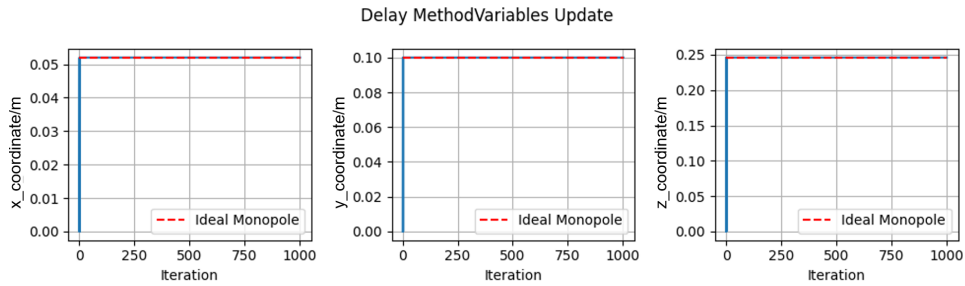


Figure 14: Update curves of the coordinate positions using the delay method for the ideal simulated monopole model.

Figure 15 and 16 show the coordinate position update curves for the WEM using the TFE standard and the weighted order  $\bar{N}$  standard, respectively. To further illustrate the localization effect, related parameter curves are also presented: for the WEM TFE case, the TFE value at the localized center is shown for each iteration; and for the WEM  $\bar{N}$  case, the power distribution across each order at the center in each iteration is displayed.

The results show that the WEM TFE method's output fluctuates around the intended target position and does not achieve noticeable stability within the first 10 iterations. The TFE curve indicates a decrease in value with each iteration. However, the initial TFE value is around -60 dB, which is already considered a credible result for NFS HFI. The accurate fit despite an imperfect or incorrect expansion point is due to coefficient overfitting. This suggests that, given a measurement surface constructed from a limited number of points, the nonlinear error from an incorrect expansion point selection can be compensated by adjusting the distribution across different orders. Nevertheless, theoretically, the TFE value should be lowest and closest to zero at the correct acoustic center. The observed fluctuations in this case also results from an overly large update step in the cost function's gradient descent, causing the solution to oscillate around the minimum. The cost functions are represented below.

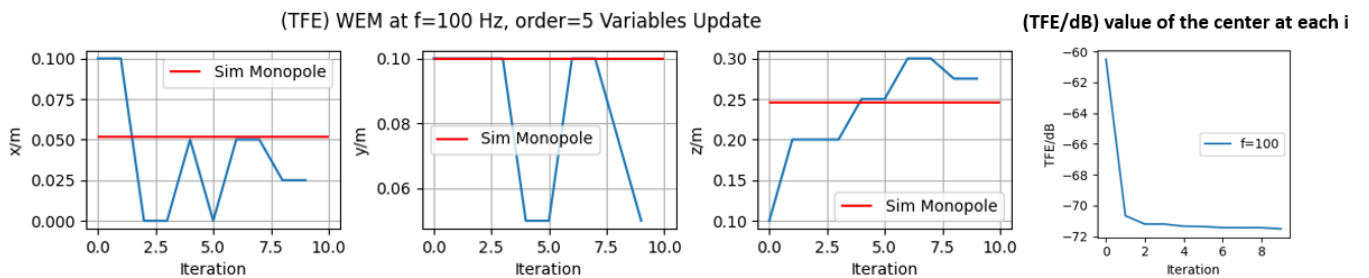


Figure 15: Update curves of the coordinate positions using the WEM in TFE standard for the ideal simulated monopole model.

In the case of the simulated monopole, unlike TFE-based standard results, the results based on the  $\bar{N}$  criterion are stable, reflecting changes in the power distribution. The optimization process

reduces the power in higher orders and concentrates it in the order 0 radiation. It is consistent with the setup because the monopole has the same radiation pattern as the SHF in order 0, though with a different amplitude [7].

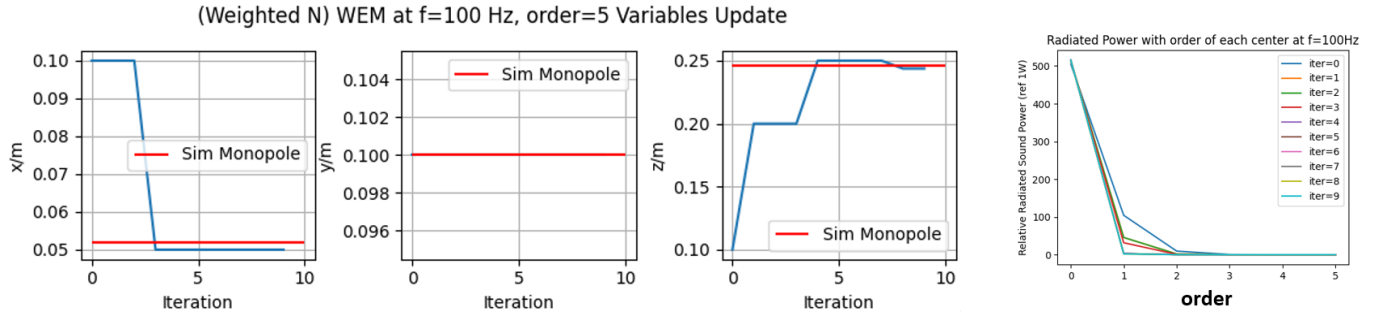


Figure 16: Update curves of the coordinate positions using the WEM in  $\bar{N}$  standard for the ideal simulated monopole model.

To better analyze and understand the WEM results, Figure 17 presents the spatial cost functions for both standards-based results of the cross-section at  $x = 0.052m$ , which corresponds to the target  $x$  position, across different maximum expansion orders in the same observation scale. The first row displays the TFE-based results. It is evident that this parameter is sensitive to the expansion order: the higher the maximum expansion order, the larger the flat valley area in the cost functions. As explained earlier, with an increase in the maximum order, the compensation effect becomes stronger, leading to a higher tolerance for an imperfect expansion point and making it more challenging to accurately localize the acoustic center.

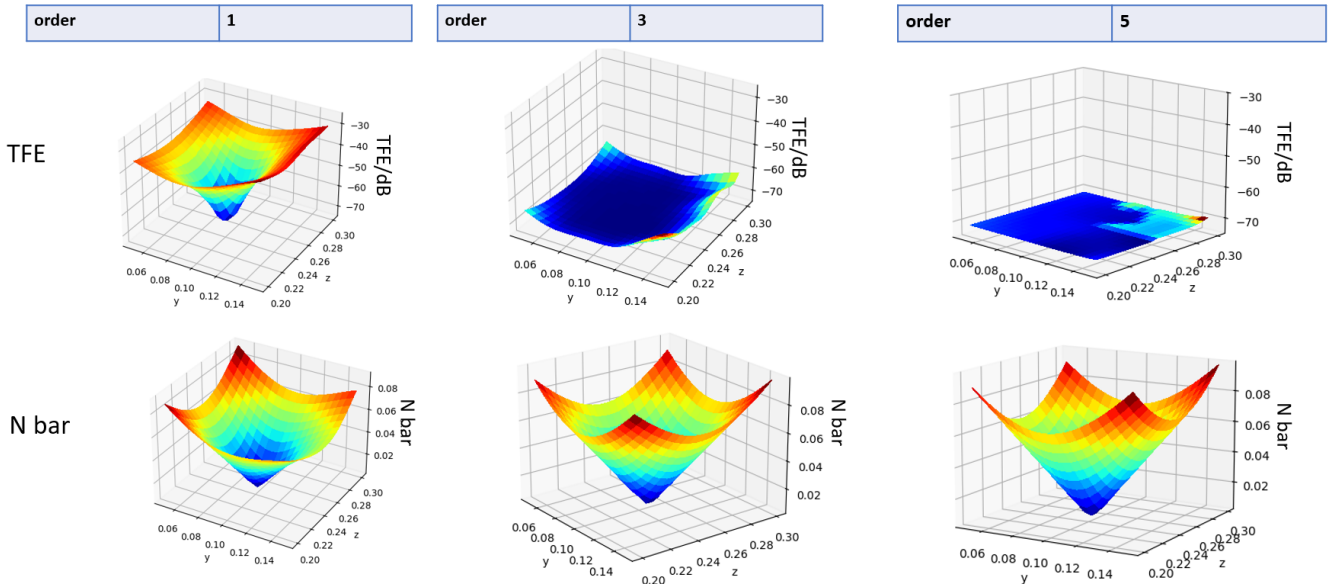


Figure 17: Cost functions of WEM in TFE-based standard (first row) and  $\bar{N}$ -based standard (second row) across different maximum expansion orders at the cross-section  $x = 0.052m$ .

Aside from the effects of inappropriate expansion points, real measurement conditions present additional challenges. Overfitting dedicated to background noise and room effects can result in inaccurate localization. Furthermore, the relationship between the actual radiated power field and

the distribution of measurement points can introduce measurement biases, further affecting the accuracy of localization. The following more complex examples illustrate these issues in detail.

The second row shows the  $\bar{N}$ -based cost functions, where the function variable is the weighted order rather than the error. Since the cost functions in both rows are observed in the same area, the  $\bar{N}$ -based results correspond to the TFE results in the first row. All the TFE values are below -20 dB, indicating credible fits but also overfitting. It can be observed that the cost functions are not sensitive to the expansion order and can localize the acoustic center because the expected outcome, where only the order 0 SHF radiates, corresponds to the minimum point. Additionally, the minimum  $\bar{N}$  value is also close to 0, which is consistent as the setup.

The simulated monopole provides the simplest and most straightforward scenario for exploring acoustic center localization. This example highlights basic localization outcomes, particularly under conditions of overfitting. The results demonstrate that both the delay method and the WEM  $\bar{N}$ -based method can achieve accurate localization. In contrast, the WEM TFE-based method exhibits instability due to overfitting compensation, although its optimization process does reach a lower TFE, resulting in a better fit. Theoretically, faster fitting is possible. The delay method requires only a minimum of four measurement points, with a relatively short update process. For WEM, using order 1 suffices for optimization, reducing the number of required measurement points and significantly cutting down on time costs. However, real-world measurements must consider robust factors such as background noise and latencies for the active sound sources. Further research is needed to develop more time-efficient optimization processes and to establish rules that account for different case classifications.

As previously mentioned, the low-frequency behavior of some multi-way compact loudspeakers, as well as omnidirectional subwoofers and woofers, can be effectively simulated using the monopole model. From a research perspective, localizing the acoustic center using the Klippel NFS can validate and extend the understanding of how the acoustic center position varies with frequency in different enclosures, as explored by Vanderkooy [2] and Samuel D. Bellow [6]. Accurately determining the acoustic center position is crucial for obtaining the correct order distribution of a sound field, which poses both a goal and a challenge for the WEM TFE method. However, the simulated monopole case is too simple to fully explore this objective. Therefore, more comprehensive discussions will be presented in subsequent examples.

### 7.3 Simulated Line Array - Advanced Discussion

In real-world scenarios, many sound sources exhibit complex directivity patterns that cannot be adequately represented by simple models like the monopole. Examples include vented box systems, line arrays, and Distribution Mode Loudspeakers. Additionally, due to diffraction effects, the sound field at high frequencies becomes complicate. Accurately describing these complex sound fields requires higher-order SHFs, where the power distribution is neither confined to a single order nor solely concentrated in order 0.

This section presents the localization results for a sound field generated by two monopoles in opposite phases at different frequencies. The analysis explores whether the outcomes are reasonable and discusses the inspirations for achieving the research objectives outlined in Section 7.1. The tables in Figure 18 provide details on the simulated line array and the configuration parameters for the two optimization methods.

|                      |   | Delay Method            |  |
|----------------------|---|-------------------------|--|
| Parameters           | Setup Value   |                         |  |
| Source Type          | Ideal Dipole  | WEA Iteration           | 10,000                                 |
| Source Position      | (0.052,0,0.343) ->Power=100dB<br>(0.052,0,-0.343)->Power = -100dB | steps                   | (1,1,1)                                |
| Localization Method  | Delay Method : TDoA+LMS<br>WEA : TFE<br>WEA : Weighted Order      | Method                  | First TDoA, then LMS                   |
| Initial Point        | (0,0,0)   | Frequency               | [63,125,250,500,1k,2k,4k,8k,<br>16k]Hz |
| Point Number         | 500   |                         |  |
| Measurement Cylinder | Cyl 1 : (r=0.5,h=0.8)<br>Cyl 2 : (r=0.6,h=0.9)                    |                         |  |
|                      |   | WEA Method              |  |
|                      |   | Iteration               | 10                                     |
|                      |   | Initial Steps           | 0.05m                                  |
|                      |   | Maximum Order           | 5                                      |
|                      |   | Frequency               | [63,125,250,500,1k,2k]Hz               |
|                      |   | Point Number per octave | 1                                      |

Figure 18: Experiment configuration of the simulated line array grouped two monopoles in opposite phase.

Figure 19 presents the far-field sound field extrapolated using NFS visualization, expanded from the midpoint between the two monopoles. This provides the reference fields. It can be observed that at low frequencies, the sound field resembles a dipole pattern, with side lobes becoming more prominent above 500Hz. Due to the limitations in the number of measurement points and the expansion order, the field is underfitted and inaccurate above 2kHz. The turning frequency corresponds to the wavelength equal to the distance between the two monopoles  $d$ . In this case, the NFS HFI results are not reliable.

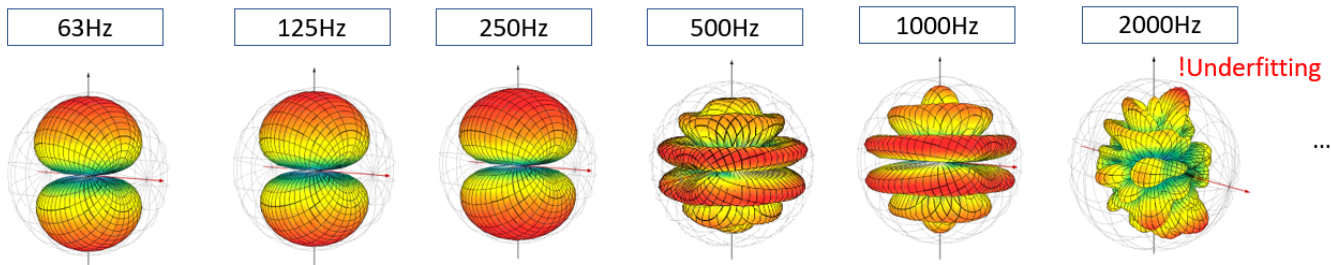


Figure 19: Representation of the low frequency and middle frequency sound fields expanded with the expected acoustic center (the middle point of the two sources) by NFS Visualization.

### 7.3.1 Delay Method Point Selection

The delay method is initially employed for localization. In addition to the measurement sets listed in the configuration table, results using measurement points only on the top and bottom circles are also presented for analysis and comparison. Figure 20 shows the localization results at different frequency of the different measurement sets. When using the same representation scales for the same axis, it becomes evident that the results obtained with the top and bottom circle measurement points are more concentrated around the expected positions. The likely reason for this improvement is the interference between the two monopoles, which causes some measurement points to be placed in the

sound field's dark zones, where the amplitude is close to zero. These low-amplitude results are not meaningful and introduce confusion to the algorithms.

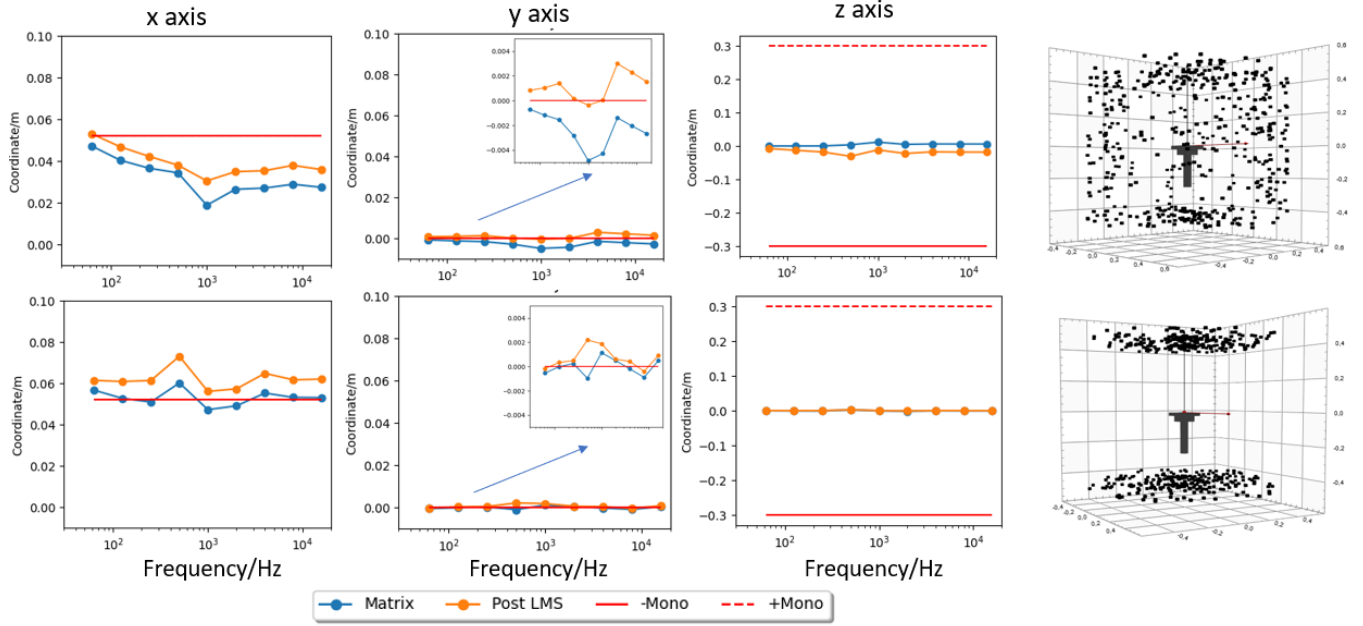


Figure 20: Optimized acoustic center coordinates with frequencies using the delay method for the simulated line array with different measurement point sets.

By limiting the measurement points to the top and bottom circles, the portion of zero-amplitude points is reduced, leading to more accurate localization. Moving forward, a result selection process should be implemented to exclude measurements with near-zero amplitudes, further improving the accuracy of the localization.

### 7.3.2 Overfitting and Appropriate Distribution of Coefficient

This section discusses the WEM TFE optimization results and further explores the relationship between overfitting and the search for an appropriate distribution of coefficients. Figures 21 and 22 compare the final localization results of WEM using TFE-based and  $\bar{N}$ -based standards, respectively, against the source positions. These comparisons use an expansion order of 10. It is important to note that the HFI results above 2 kHz are not reliable due to underfitting. The results at exactly 2 kHz are further examined within the WEM TFE framework to explore the potential for achieving a good fit. Additionally, the figures display the TFE and  $\bar{N}$  values for each iteration's center, providing insights into the optimization process.

Notably, at 2 kHz, the TFE value of the final iteration remains above -10 dB, indicating significant underfitting, meaning the sound field is not adequately represented, and the result is unreliable. At other frequencies, the TFE values gradually decrease. The localized center coordinates are close to the expected position (the midpoint of the source array) but generally deviate by several centimeters, which is acceptable distance. As previously discussed, in overfitting scenarios, the cost function tends to be flat, leading to significant jumps around the minimum and causing the inaccuracy of the results.

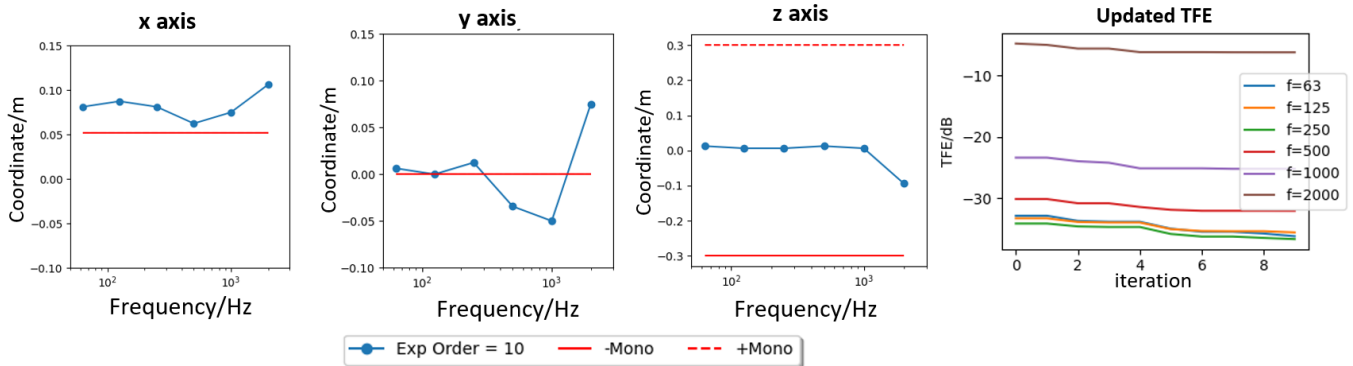


Figure 21: Optimized acoustic center coordinates with frequencies and updated TFE values for WEM in TFE-based standard for the simulated line array.

Given the underfitting observed at 2 kHz, the weighted order optimization is limited to frequencies below 1 kHz. The localization results do not reveal a moving rule for the power center in this simulation. At 1 kHz, the localization result falls outside the middle area between the sources, indicating a low  $\bar{N}$  value, but the sound field is not accurately represented, making this result unreliable.

The localization results at mid-frequency ranges are close to the expected center. Specifically, at 125 Hz and 250 Hz, the steady weighted order is closer to order 1, and at 500 Hz, the order is higher than 2, aligning well with reference fields. However, at the low frequency of 63 Hz, the localization deviates significantly in the  $x$  and  $y$  axes. This deviation is due to near-field effects and the distribution of measurement points, which lead to a local identification of the sound field. Subsequently, the WEM  $\bar{N}$  method identified an expansion point that describes the field using lower-order combinations, such as a cardioid. Therefore, the steady  $\bar{N}$  values are also useful for determining the main power-radiating order.

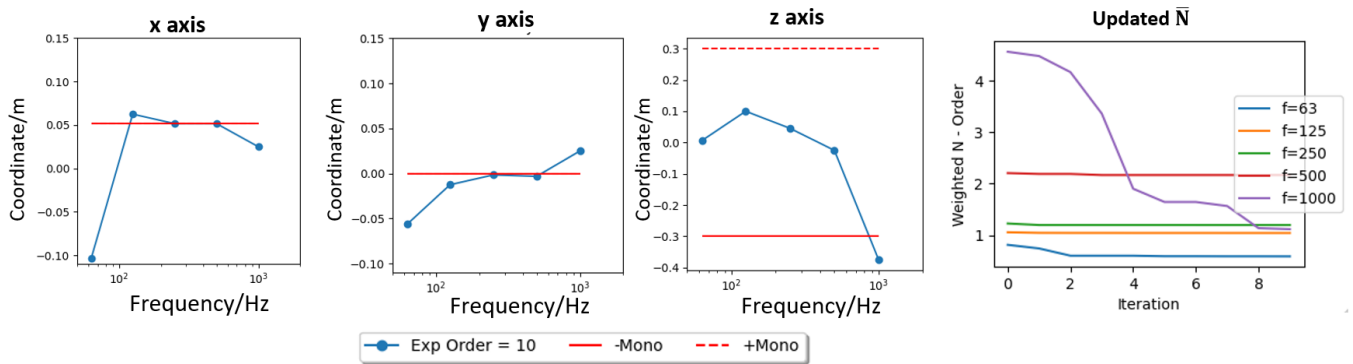


Figure 22: Optimized acoustic center coordinates with frequencies and updated weighted order values for WEM in  $\bar{N}$ -based standard for the simulated line array.

Figure 23 illustrates the TFE curves from 20 Hz to 1.5 kHz, comparing the results expanded with the initial expansion point with the centers localized using the WEM TFE method. A noticeable improvement in fitting, with an average reduction of 5 dB in TFE, suggests a better match between the reproduced and the actual sound field.



Figure 23: TFE curves of the simulated line array expanded from the initial point and the localized acoustic center, respectively.

However, except the previous discussions, due to the finity of the resolution and distribution of the measurement set and also the existence of the noise in the real measurements, the optimization result may not correspond to the most appropriate order distribution of the given sound field. Proper expansion order is a key to solve this problem, because the cost functions of the good fit has a larger derivation increment and take the main power-radiated order SHF into the first account and the most appropriate acoustic center has an obvious advantageous TFE values.

Figure 24 presents a discussion example at 500 Hz. The first subfigure illustrates the power distribution of the expansion result at the expected acoustic center. Generally, the primary radiated SHFs are in orders 1, 3, and 5, which aligns with the dipole-like sound field of this line array. The first row shows the localization results using expansion orders [1, 2, 3, 4, 5, 10], while the second row depicts the TFE cost functions for cross-sections along the expected  $x$ -axis.

The results for orders 3 and 5 align with expectations, reflecting the higher power radiated in these orders. However, the mislocalization observed in order 1 is an example of a trap. Although order 1 also radiates significant power and its cost function exhibits a large gradient, the majority of the sound field cannot be accurately captured with just order 1. This leads to a cost function with misleading subminima across the 3D space, which adversely affects the localization results. The intermediate order 2 and 4 has the same affects as the overfitting but for compensating the not included main power, which can be regarded as local overfitting.

As mentioned before, one potential solution for identifying the optimal expansion order is to correlate it with the weighted order,  $\bar{N}$ . This parameter indicates the order of power concentration, which is related to the dominant radiated power orders that capture the majority of the sound field. For example, the optimized  $\bar{N}$  value at 500Hz in Figure22 is around 2.4 close to the order 3. However, due to the lack of firm theoretical validation and comprehensive case studies, this assumption has not yet been incorporated into the current software. This approach represents a valuable area for future research, as determining the appropriate fitting order based on  $\bar{N}$  could help reduce measurement time and improve efficiency. It is important to note that this discussion is currently relevant only in the context of overfitting scenarios.

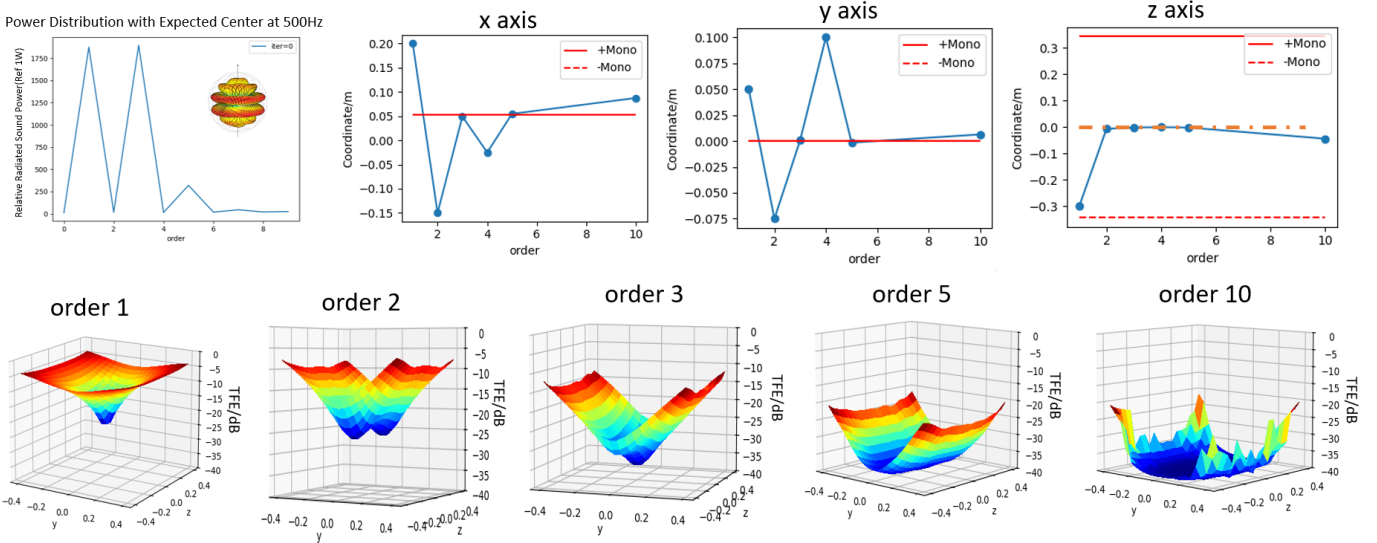


Figure 24: Representation of power distribution and localization results at 500 Hz for simulated dipoles with different maximum expansion orders (line 1) and the corresponding cost function for cross-section  $x = 0.052\text{m}$  (line 2).

### 7.3.3 Underfitting and Potential Solutions

A significant challenge with the Klippel NFS, as well as traditional sound field measurement techniques, is dealing with underfitting, which occurs when the resolution is insufficient. This section explores potential solutions to this issue. The most straightforward approach is to increase the number of measurement points to enhance resolution. However, this method presents the associated problem of extended measurement times.

Another potential solution is to use the delay method. High-frequency sound fields tend to be complex and require higher measurement resolution due to diffraction effects. However, the delay method offers an advantage in this scenario: at high frequencies, the results are more reliable because of the shorter wavelengths, allowing the measurements to approximate far-field conditions. By initially using the delay method to localize the acoustic center, the appropriate expansion point can be identified. This reduces the need for higher-order compensations and decreases the required order for a good fit.

Predicting the sufficient order is a valuable approach to addressing the underfitting problem, as it can help minimize the number of trial measurements with either redundant or insufficient measurement points. This prediction process represents a new area of research that involves examining how TFE values vary with order and frequency across different sound sources. For example, Figure 25 illustrates the TFE curves for both the simulated line array and the measured JBL Control Pro1, which will be analyzed in detail later. These functions can be modeled using linear functions or inverse exponential functions, providing a potential framework for optimizing measurement strategies.

In real measurement cases, the TFE stabilizes after a certain order due to inherent uncertainties and robust effects. In contrast, the ideal simulated model can theoretically achieve TFE values approaching negative infinity. This leads to discrepancies between the two results.

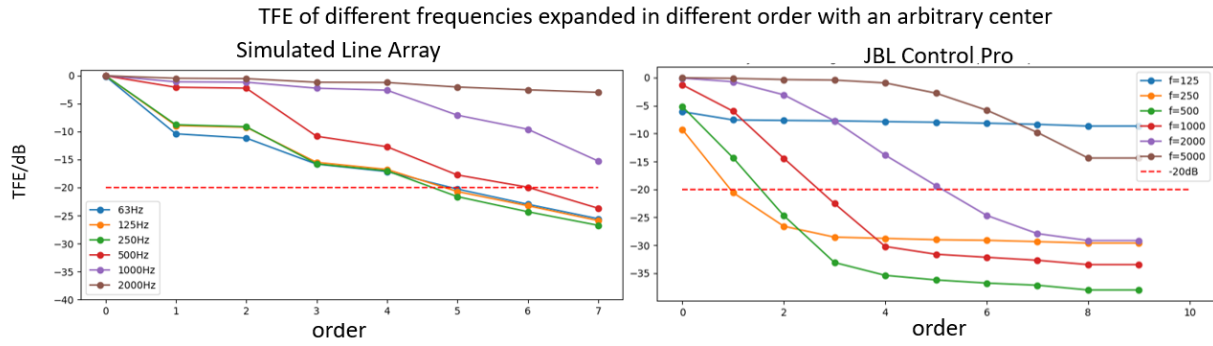


Figure 25: The TFE-order curves across the various frequencies at a reasonable arbitrary expansion point of the simulated line array and the JBL Control Pro 1.

## 7.4 JBL Control 1 Pro - Real Measurement

This section presents and discusses the localization results from a real measurement process of a 3-way passive compact vented loudspeaker, the JBL Control 1 Pro. Table 1 and Figure 26 provide detailed information about the experimental setup and the measurement configuration. It is important to note that the crossover frequency is 4.2 kHz. The SNR values across the observed frequency range exceed 40 dB, ensuring the credibility of the measurement data. Theoretically, the acoustic center is expected to be near the woofer below this frequency and shift closer to the tweeter above it.

| Nb Mesurement Point           | Tweeter Place/m | Woofer Place/m     | Vent Place/m    | Crossover Frequency/Hz |
|-------------------------------|-----------------|--------------------|-----------------|------------------------|
| 300                           | (0.07,0,0.175)  | (0.06,-0.03,0.077) | (0,-0.05,0.159) | 4.2k                   |
| Observation Frequencies/Hz    |                 |                    |                 |                        |
| [50,125,250,500,1k,2k,5k,10k] |                 |                    |                 |                        |

Table 1: Selected useful information of the JBL Control Pro and the measurement configuration.

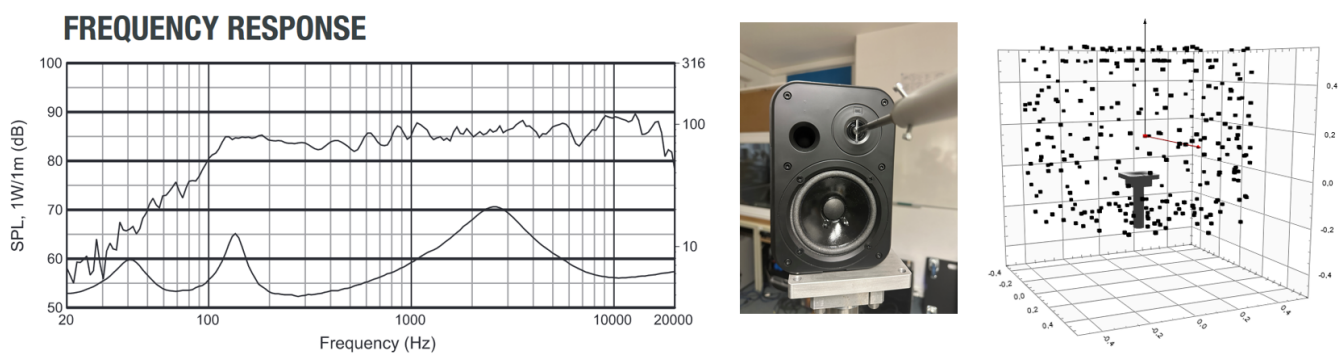


Figure 26: Representation of the official frequency response of JBL Control Pro 1 and measurement configuration.

Figure 27 illustrates the localization results obtained using the delay method. Since the Python data transferred from the NFS MDC represents raw, untreated data and low-frequency effects are

present, the delay method is applied only to frequencies above 1 kHz. The final centers identified by both algorithms generally align with expectations: at middle frequencies, the centers are positioned near the woofer, while at 5 kHz and 10 kHz, they shift toward the tweeter. Observing the  $z$  axis, it is evident that at higher frequencies, the centers are located above the tweeter's center. This shift is likely due to diffraction effects, causing the propagation center to move upward toward the edge of the speaker.

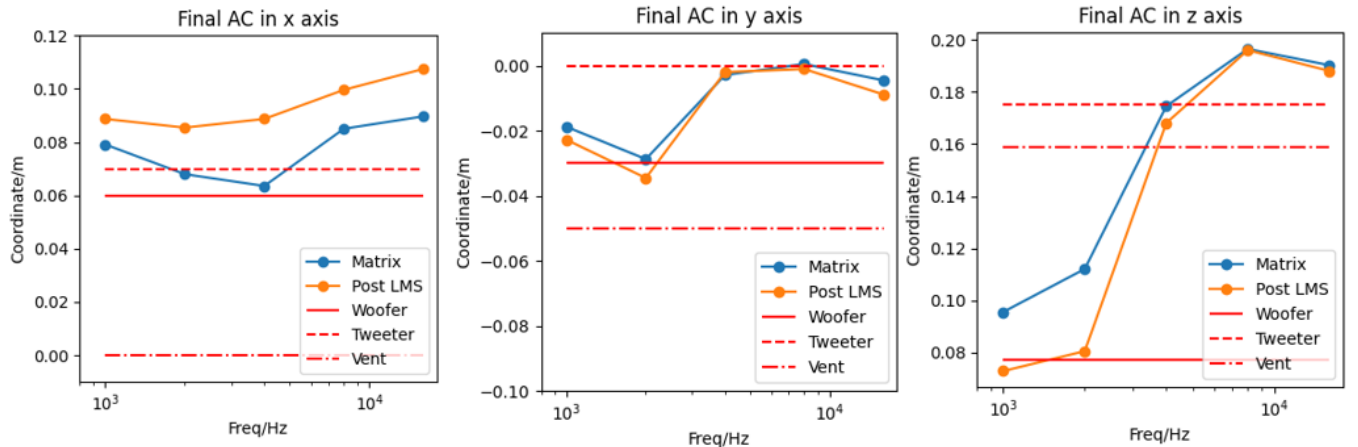


Figure 27: Optimized acoustic center coordinates with frequencies using the delay method for the JBL Control Pro 1.

Figure 28 shows the localization results of WEM in the two standards. Building on the previous cases and analyses, the current interpretation combines the results from both standards. The updated TFE curves indicate that, for frequencies below 1 kHz, the final values are below -20 dB, suggesting that the majority of the radiated power has been fitted, potentially leading to overfitting or localized overfitting. For higher frequencies, the TFE values are also below -15 dB, indicating that the fitting process is effective, though it may not encompass all radiated power. The  $\bar{N}$  values indicate that the weighted order increases with frequency. At lower frequencies, the order is close to 0, showing a monopole-like directivity pattern. The result at 10 kHz is unreliable, as it fails to accurately fit the sound field.

The centers localized using the TFE-based WEM standard float around the expected positions at lower frequencies. This instability arises from overfitting and unnecessary fitting to noise—an issue not present in the simulated cases. However, due to the high SNR maintained during measurement, the noise effect is minimal, and overall, the TFE localization results are consistent with the expected positions.

The centers localized using the  $\bar{N}$ -based WEM standard are generally reasonable, except at 10 kHz, as previously discussed. Observing the  $y$  and  $z$  axes, it is evident that the power centers shift from the vent towards the woofer and then approach the tweeter with increasing frequency. The  $x$  axis reveals an interesting trend: at low frequencies, the center remains constant and in front of the membrane, but as the frequency increases, it moves from the front of the membrane and gradually aligns more closely with the source. This behavior is consistent with Vanderkooy's research on the monopole acoustic center of subwoofers. Therefore, NFS offers a valuable method for identifying the low-order acoustic center, which is crucial for studying the listening zone.

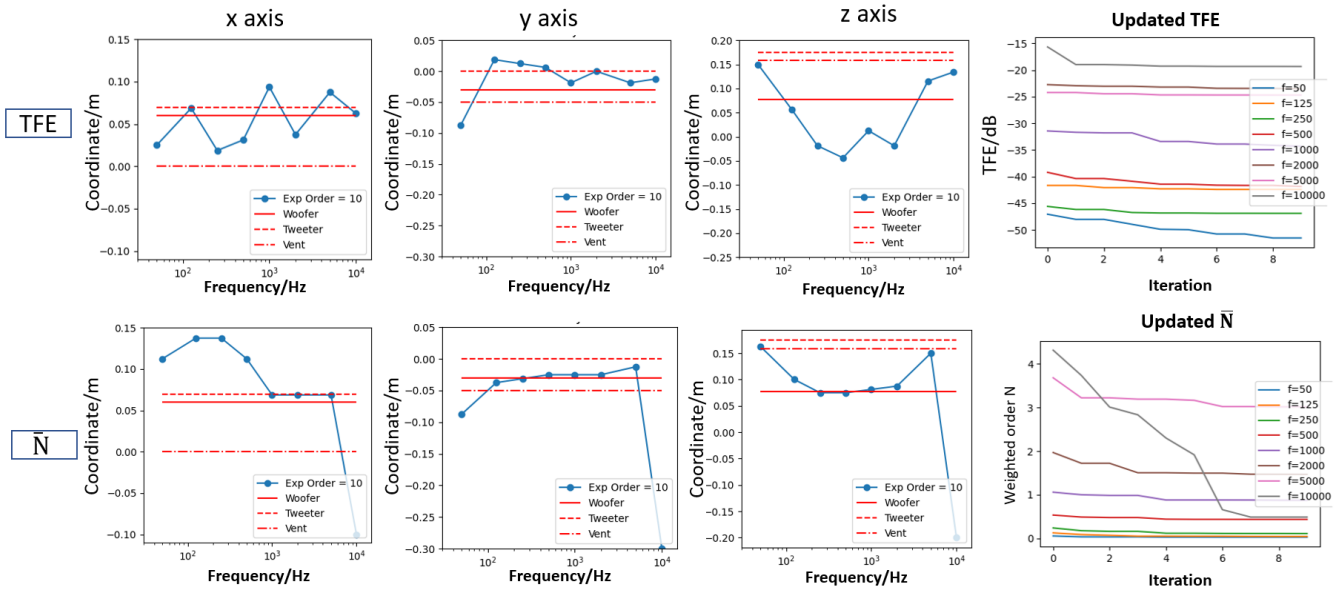
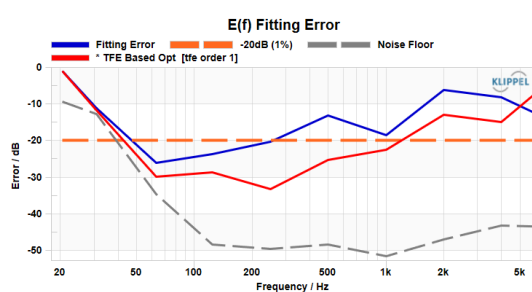


Figure 28: Optimized acoustic center coordinates across expansion order 10 and various frequencies using the WEM in TFE-based (first row) and  $\bar{N}$ -based (second row) standards, and the updated parameter values for the JBL Control Pro 1.

Based on the previous assumption, in the case of overfitting, the optimized  $\bar{N}$  values indicate the dominant radiating sound order, providing insights into the appropriate expansion order that can enhance the WEM TFE results. In this real measurement scenario, the optimization results based on this assumption are presented for frequencies below 6 kHz. Figure 29a shows the TFE curves, where the blue curve represents the initial expansion point at the tweeter position, and the red curve represents the WEM TFE optimized acoustic center. Both curves use the expansion order provided in the table of Figure 29b, which is determined by the updated  $\bar{N}$  results in Figure 28. The fitting quality of the red curve shows improvement over the blue one. The localized acoustic center remains near the woofer position for frequencies below 5 kHz and shifts closer to the tweeter at 5 kHz. Although the data is not displayed here due to time constraints in the integration process, it can be concluded that combining both standards offers a promising solution to achieve the desired objectives.



(a) Record of automated optimization processes and operations in dB-Lab at one frequency.

| Frequency/Hz | Expansion Order |
|--------------|-----------------|
| 50           | 1               |
| 125          | 1               |
| 250          | 1               |
| 500          | 1               |
| 1000         | 3               |
| 2000         | 3               |
| 5000         | 5               |

(b) Record of localization center history of a series of frequencies.

Figure 29: Running record of the WEM optimization processes.

## 8 Conclusion

This project explored two methods for acoustic center localization, along with their sub-algorithms, and developed an associated software system for simulating and analyzing real sound sources using the Klippel Near Field Scanner, dB-Lab software, and the provided modules. The two methods, namely the delay method and the wave expansion method (WEM), were examined based on different definitions of the acoustic center.

During the internship, various sound sources were measured and localized, with the report providing a detailed analysis of three specific examples. The localization results generally met expectations, but the inherent complexity of the sound field, the presence of robust factors, and the limitations of near-field holographic measurements posed challenges. While the project did not result in a fully developed system for commercial use, it successfully identified existing problems and potential solutions.

The delay method demonstrated the potential for fast and accurate localization. However, challenges remain, particularly in eliminating the influence of uncertain latency and selecting the optimal points for further optimization. Additionally, in-situ measurements were significantly affected by room acoustics. Although the Klippel NFS offers cutting-edge in-situ measurement techniques, the system currently lacks the functionality to fully process and extract the data. Future work should focus on integrating point selection algorithms and validating the method's effectiveness for active loudspeakers with added latency.

On the other hand, the WEM is constrained by high frequencies due to underfitting, which results from low measurement spatial resolution. Despite this, WEM can benefit from the overall post-processing capabilities of dB-Lab NFS, showing reliable and reasonable results across two standards. The TFE-based results align most closely with the primary goal—achieving the best fit with the lowest fitting error. However, the method's sensitivity to the setup's expansion order and background noise poses challenges, particularly in cases of overfitting. The  $\bar{N}$ -based results indicate a consistent trend with low-frequency acoustic center rules derived from BEM theories, though there remains a risk of non-fitting. Advanced algorithms tailored to address these issues are needed.

Looking forward, a more comprehensive algorithm is anticipated from the WEM perspective, one that combines the two standards, enabling acoustic center localization with optimal order distribution and minimal fitting error. Moreover, the development of faster computational software that can be integrated into dB-Lab is also desirable.

In addition to working on an interesting and forward-looking project, Klippel GmbH provided a supportive and professional environment. I gained not only project-specific knowledge but also insights into becoming a competent engineer. I learned about scientific system development processes and systematic team collaboration, which will benefit my entire career. Furthermore, the colleagues were friendly and innovative, making my experience at the company enjoyable and rewarding.

## References

- [1] Wolfgang Klippel, Christian Bellmann, “Holographic Nearfield Measurement of Loudspeaker Directivity,” *Audio Engineering Society Convention Paper*, October 2016.
- [2] John Vanderkooy, “The Acoustic Center: A New Concept for Loudspeakers at Low Frequencies,” *Audio Engineering Society Convention Paper*, October 2006.
- [3] A. D. Pierce, *Acoustics*. Acoustical Society of America through American Institute of Physics, 1989.
- [4] Mario Di Cola, Paolo Martignon, and Merlijn Van Veen, “Effects of Acoustic Center Position in Subwoofer,” *Audio Engineering Society Convention Paper*, October 2017.
- [5] Samuel D. Bellows, “Acoustic Directivity: Advances in Acoustic Center Localization, Measurement Optimization, Directional Modeling, and Sound Measurement Optimization, Directional Modeling, and Sound Power Spectral EstimationPower Spectral Estimation,” *Theses and Dissertations of Brigham Young UniversityBrigham Young* , pp. 6–42, June 2023.
- [6] Samuel D. Bellows and Timothy W. Leishman, “Acoustic source centering of musical instrument directivities using acoustical holography,” *Acoustical Society of America*, December 2020.
- [7] E.G.Williams, *Fourier Acoustics*. ACADEMIC PRESS, 1999.
- [8] Klippel GmbH, “Klippel E-Learning Hands-On Training 8: Measurement of Loudspeaker Directivity,” *Klippel E-Learning Training*, December 2018.
- [9] “Near field scanner system (nfs).” <https://www.klippel.de/products/rd-system/modules/nfs-near-field-scanner.html>. Klippel GmbH Website.
- [10] M. URBAN, C. HEIL, C. PIGNON, C. COMBET, AND P. BAUMAN, “The Distributed Edge Dipole (DED) Model for Cabinet Diffraction Effects,” *AES Papers*, 2004.
- [11] Wolfgang Klippel, “Active Control of Sound and Vibration V4: Linear Adaptive Contol, LMS Algorithm Example: Echo Cancellation, Hands-free Telephone,” *Lecture “Active Control of Sound”*, 2021.
- [12] “Qr decomposition.” [https://en.wikipedia.org/wiki/QR\\_decomposition](https://en.wikipedia.org/wiki/QR_decomposition). Approximate solution.
- [13] Klippel GmbH, “Klippel Automation 212.699,” , 2023.

## Appendix

### A Method Validity

#### A.1 Ideal Source

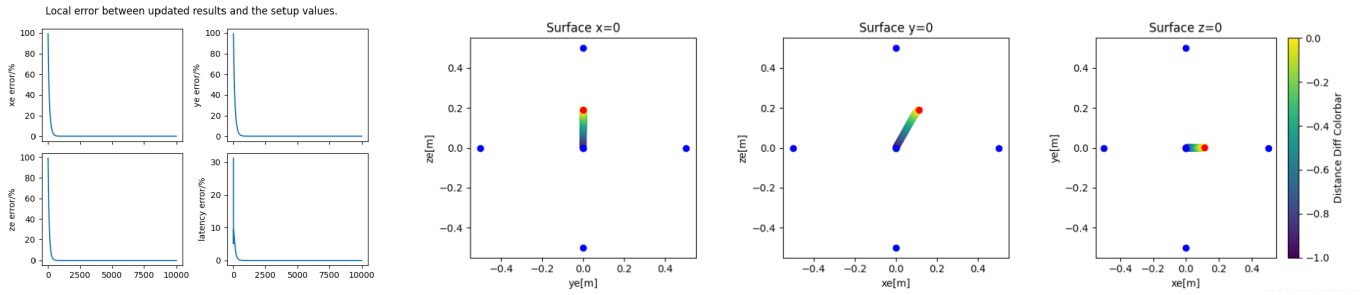
The ideal sound source simulation data is constructed and used to localize the known center using both delay-based and wave-expansion-based methods. For the delay-based method, the simulated measurement time is calculated by dividing the distance by the sound speed, as shown in the right part of Figure 9. For the wave-expansion-based method, the simulated frequency response of the measurement points is calculated using Equation (7). The precise experiment setup is shown in Table 2.

It can be seen that due to the calculation advantage of DALM, the results can be obtained immediately. In contrast, each iteration of the wave-expansion-based method takes longer. Here, one easy-localized experiment with 5 iterations is performed. Since it is not influenced by latency, there is no specific set time.

|                | Source Position/mm   | Latency/ms                   | Update Step        |
|----------------|----------------------|------------------------------|--------------------|
| Delay Method   | (111,1,189)          | 1                            | (100,10,10,0.01)   |
| Wave Expansion | (10,0,-50)           | 0                            | Init:(0.1,0.1,0.1) |
|                | Iteration Number     | Measurement Type             | Localize Result/mm |
| Delay Method   | LMS: 1000;DALM: None | 6 on axis points             | Both: (111,1,189)  |
| Wave Expansion | 5                    | 10 random points on cylinder | (100,0,-50)        |

Table 2: Experiment setup and the localization results of the simulated ideal source.

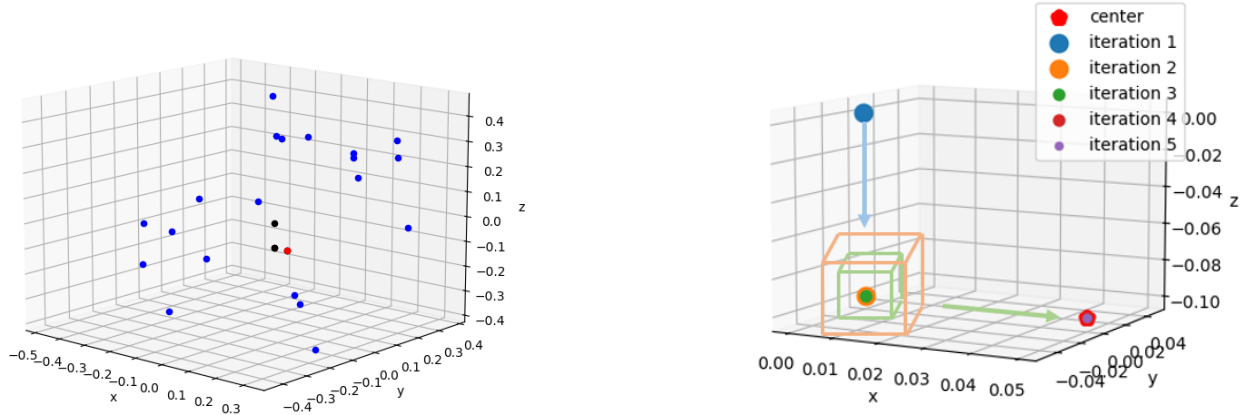
Figures 30a and 30b represent the local mean squared errors for all variables and the 2D convergence process projection, respectively. In these figures, the red point indicates the set center, the blue points are the measurement points, and the color map points show the result of each iteration (the same configuration for the 2D projection plot is used later). Without noise, the LMS algorithm can straightforwardly converge all variables. From Table 2, it can be seen that both the LMS and DALM algorithms can accurately localize the center without error. This confirms the effectiveness of the delay-based method.



(a) Local mean squared error (b) 2D projection of the converging process to the acoustic center of the  
of the LMS algorithm. LMS algorithm.

Figure 30: Updating curve of the delay method validity.

The converged results of the 3D wave expansion method are shown in Figure 31a. In this figure, the red point indicates the set center, the blue points are the measurement points, and the black points represent the result of each iteration (the same configuration is used later for the 3D plot). The zoomed and colored iteration process details are shown in Figure 31b. The results of iterations 2 and 3 are the same; therefore, the update increment is reduced to increase localization accuracy. The wave expansion method successfully finds the set acoustic center, confirming its effectiveness.



(a) 3D result plot for the ideal source in the  
wave-expansion method.

(b) Zoomed results of each iteration with  
the updating path.

Figure 31: Updating processes of the WEM for the method validity.

## A.2 Noised Monopole Source

The experiment setup of the simulated noised monopole in the delay method is clarified in Table 3. With the sound source closer to the one in the real world, the localization process follows the left part of Figure 9: calculating the delay time by averaging the group delay response. The results shown here is the absolute errors between the fitting outcomes and the setup values for the two algorithms with different measurement setups, respectively. The latency error is expressed by multiplying the sound speed to keep the same unit as the distance. Firstly, the results of the different measurement sets are compared for each algorithm of the delay method, respectively. Then, the two algorithms are compared with each other.

Figure 32 shows the results with different measurement setups, respectively. More measurement points or special principles for points taken don't show the advantages in the localization accuracy for both algorithms. For the more complex sound sources synthesized by higher-order SHFs, the points at the node may be useless due to the low amplitude value. The amplitude check function should be added to the method application.

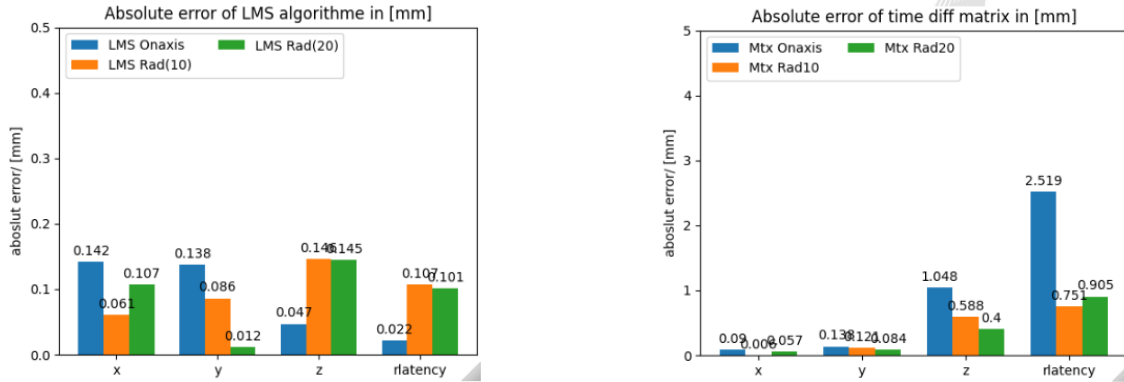


Figure 32: Absolute error result of the LMS and the DALM algorithms in 3 measurement point sets for the simulated noise monopole source, respectively.

The algorithm result comparison for different coordinates is shown in Figure 33. It's difficult to draw a definite conclusion about the advantages of each method because they all can achieve lower absolute errors. This is because of different operational mechanics. The LMS algorithm evaluates outcomes by adding the fitting situations of all points, thereby giving the final result dependent on the average noise case. On the other hand, DALM derives from the parameter differences between pairs of points. The algorithm presents outcomes based on the averaged noise differences.

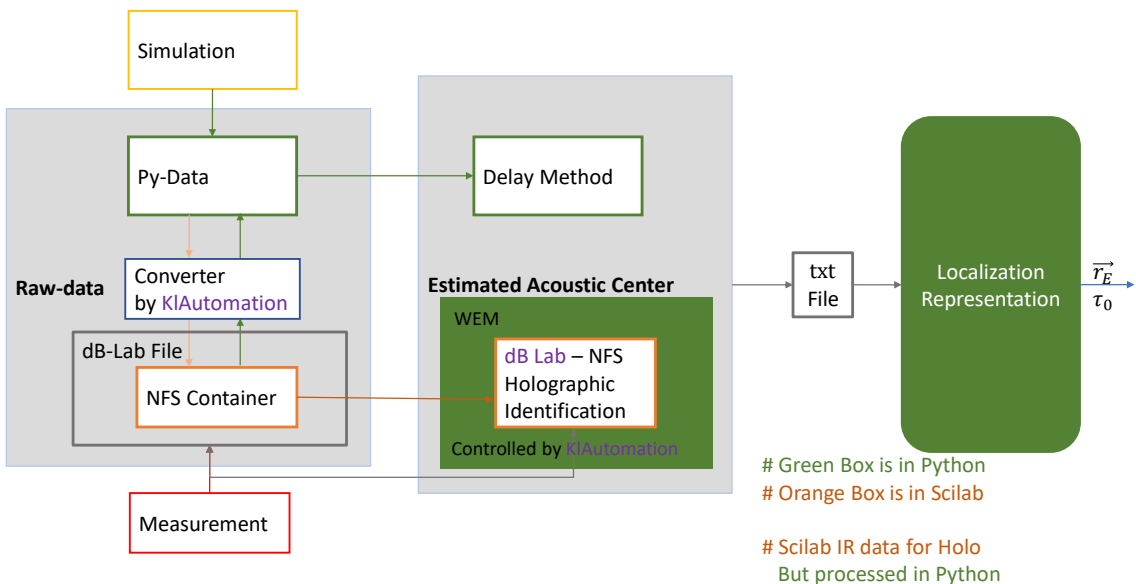
In this case, employing a combination of algorithms provides a more rigorous solution. Because the matrix method is calculated fast, experiments can be initially implemented using the DALM method and then further refined with the LMS algorithm. Generally speaking, an error of less than 1 mm is acceptable, which is one-third of the measurement microphone diameter.

## B System Running Processes

The general structure for running the experiment system processes and the explanation have been represented in the following pages. The example codes and corresponding process information are also shown.

# Acoustic Center Localization Programme Explanation

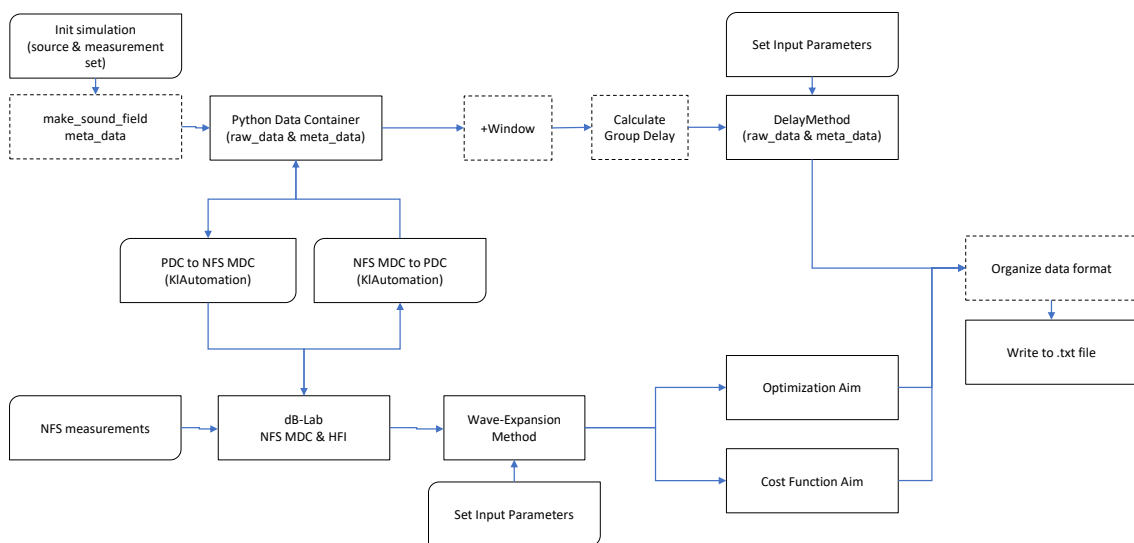
## General Structure



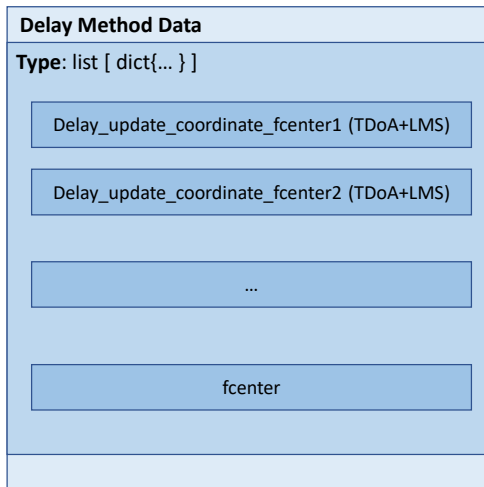
- Run

- Plot

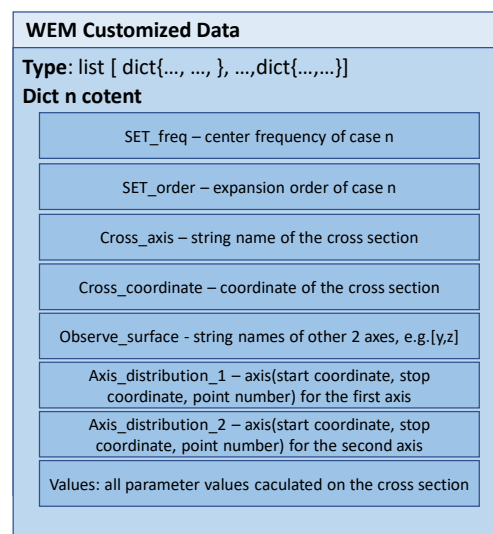
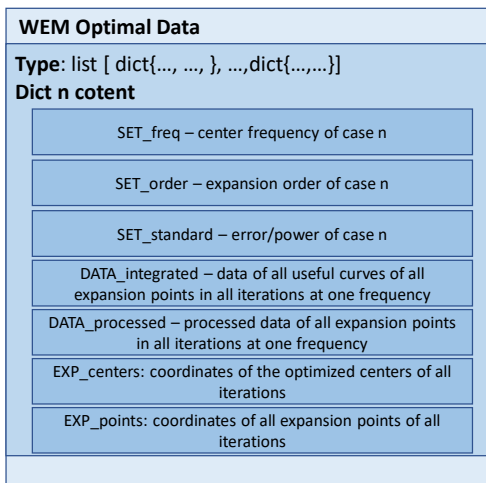
## Run – Programming Structure



## .txt File restore format – Delay Method



## .txt File restore format – WEM Optimized and Customized (Customized )



## Simulation Preparation

### Configuration– Code Example - Cylindrical Measurement Set

```
# Generate Sound Source List
set_center1: Coordinate = Coordinate(,,)
...
set_centern: Coordinate = Coordinate(,,)
n_meas : int =
latency : float =
# Generate a monopole.
s1: SoundSource=
Monopole(position=set_center1)
...
sn: SoundSource =
WhiteNoise(position=set_center1)
sn.power =
sn.SNR =

source_list: list[SoundSource] = [s1, ...,
sn]
```

```
# Generate measurement point set
r_cyl1, r_cyln = 0.8, 0.9
h_cyl1, h_cyl2 = 1.5, 1.6
pg = PointGenerator(seed=True,
constant=1)
cds1: list[Coordinate] =
pg.randpoints_cyl(n_meas, r_cyl1,
h_cyl1)
cds2: list[Coordinate] =
pg.randpoints_cyl(n_meas, r_cyl2,
h_cyl2)
cds = cds1
for cd in cds2:
    cds.append(cd)
```

## Data Container Preparation

```
"""Simulation PDC"""
db_path_str: str = r
container, faxis = sim_container_create(source_list, cds, db_path)

"""Measurement PDC""",
db_path_str: str = r
container, faxis = meas_container_create(db_path_str)
```

## Delay Method– Code Example

### Delay Method– Code Example

```
"""---Delay Launch and Run---"""
file_path = r
delay = DelayMethod(
    container=container,
    file_path=file_path,
    faxis=faxis,
    fcenter=[],
)
delay.run_delay_method()

"""---Output---"""

=====META DATA=====
f=50 turn begins.
----Finished calculating the averaged group delay time.----

----Matrix Start----
----Matrix Finished----
----LMS Start----
Finished
----LMS Finished----
----Delay Method Info----
Center Frequency: 50Hz.
Average Range: 1 octave.
-----

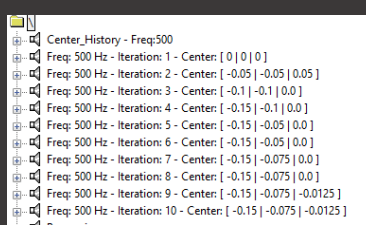
TDoA Center: (-0.0182,0.0005,0.0126)m.
-----
Update Step: (mux,muy,muz) = (1,1,1).
Init Center: = (-0.0182,0.0005,0.0126)m.
Iteration Number: 10000
-----
Delay Method Center: (-0.0268,-0.0163,-0.0553)m.
```

## Wea Optimal– Code Example

```
"""---WEA Optimal Launch and Run---"""
db_path_str: str =
file_path: str =
container, faxis = meas_container_create(db_path_str)
wea = WeaMethod(
    container=container,
    db_path_str=db_path_str,
    file_path=file_path,
    init_step=,
    init_exp_center=Coordinate(, , ),
    exp_fcenters=[, ],
    exp_order=,
    iter_num=,
    standard="error" / "power",
)
wea.run_wave_expansion_optimal()

"""---Output---"""

=====META DATA=====
---- Wave Expansion Method Initial Info----
Init Expansion Step: 0.05m.
Init Order: 3.
Init Expansion Center: (0,0,0)m.
Iteration Number: 1
TFE Center Frequency: [1000]Hz.
Average TFE Range: 1 octave.
Standard of update is error
-----
----Wave Expansion Start----
----Wave Expansion Start, f: 1000----
Iteration 1 Finished
-----
----DATA READY----
Data written to C:/Users/yliu/Experiment set/Example\wem_optimal_test.txt successfully.


```

## Wea Customized – Code Example

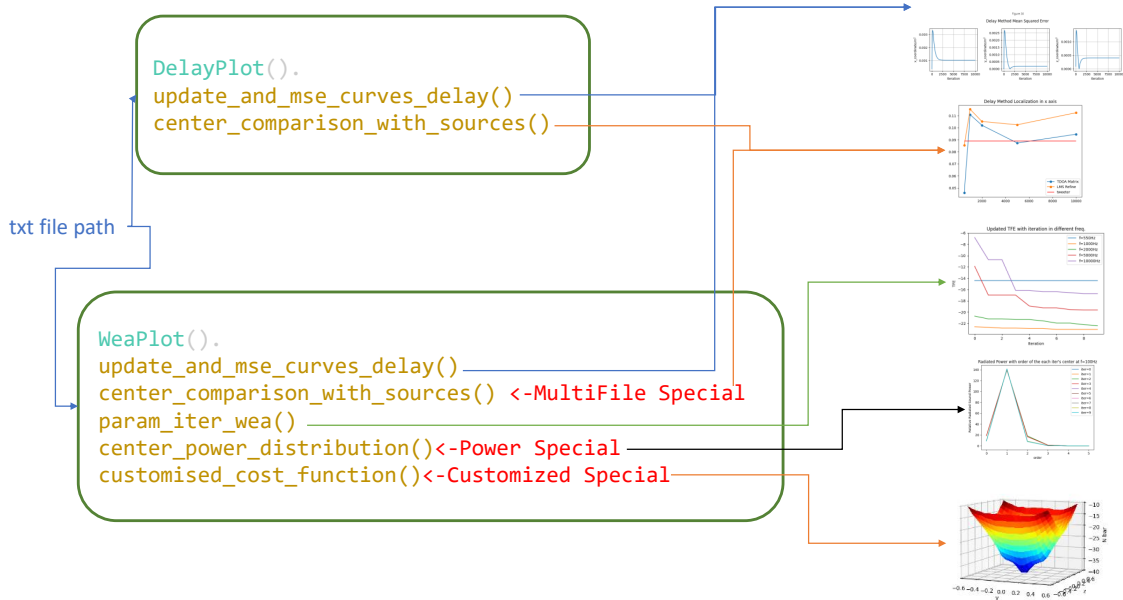
```
"""---Sim WEA Customized Setup---"""
db_cust_path_str: str = r
file_path: str = r
container, faxis = meas_container_create(db_cust_path_str)
wea = WeaMethod(
    container=container,
    db_path_str=db_cust_path_str,
    file_path=file_path,
    init_step=,
    init_exp_center=Coordinate(, , ),
    exp_fcenters=[],
    exp_order=,
    iter_num=,
    standard ="error"/ "power",
)
wea.run_wave_expansion_customized(
    cross_cd=("x", 0.052),
    axes=["y", "z"],
    l1=(-0.4, 0.4, 2),
    l2=(-0.4, 0.4, 2),
) ##An example
```

```
"""---Output---"""

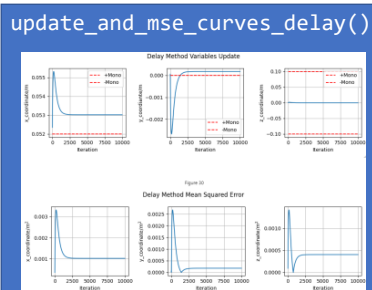
Iteration Number: 1
TFF Center Frequency: [500]Hz.
Average TFF Range: octave.
Standard of update is error
-----
Observe the yz surface, at x=0.052m
----Wave Expansion Start-----
-----
-----DATA READY-----
Data written to C:\Users\yliu\Experiment set\Example\wem_customized_test.txt successfully.
```

PLOT

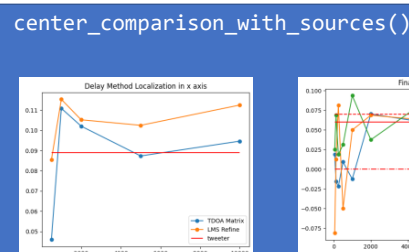
## General Plot



## Plot Explanation 1



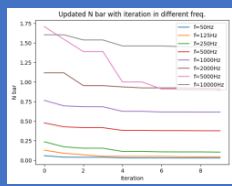
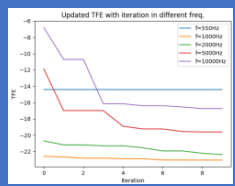
The updated coordinates and the mean square error(MSE) related to the expected acoustic center varying with the iteration. (Both Delay and WEA)



The comparison between the final localization result and the expected center position in one axis varying with the frequency.  
(Both Delay and WEA Optimal, WEA Optimal can plot multi orders file.)

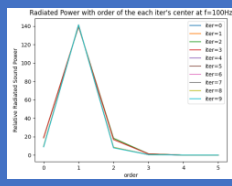
## Plot Explaination 2

param\_iter\_wea()



The criterial parameter values (TFE/Nbar) of the optimal center at each iteration in each frequency.  
(Only WEA Optimal)

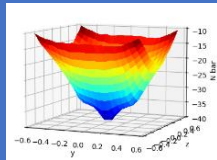
center\_power\_distribution()



The power distribution of the optimal center at each iteration in one specific frequency, but all frequencies' results are given at the same time.  
(Only WEA Optimal Power)

## Plot Explaination 3

customised\_cost\_function()



The spatial cost function at one cross sections.  
(Only WEA Customized)

## Run Code Structure

| WeaPlot()  |
|--|
| file_path  |
| update_and_mse_curves_wea()  |
| param_iter_wea()   |
| center_power_distribution()  |
| customised_cost_function( <span style="background-color: #d9e1f2;">standard</span> ) |
| center_comparison_with_sources()   |

| DelayPlot()                 |
|-----------------------------|
| file_path                   |
| update_and_mse_curves_wea() |
| param_iter_wea()            |

## Delay Method– Code Example

### Delay Method– Code Example

```
"""---Delay Method Plot Example---"""
file_path: str = r
delay_plot = DelayPlot(file_path=file_path)
start_point = Coordinate(, , ) #Optional
expect_centers_all_f: list[Coordinate] = [Coordinate(, , ),...]
delay_plot.update_and_mse_curves_delay(exp_acs= expect_centers_all_f)
delay_plot.center_comparison_with_sources()
```

## Wea Optimal– Code Example

```
"""---WEA Method Plot Example---"""
"""--Optimal--"""
"""One Expansion Order Case"""
file_path: str = r
start_point : list[Coordinate] = [Coordinate(, , ),...] #Optional
expect_centers_all_f: list[Coordinate] = [Coordinate(, , ),...] #Optional
wea_opt_plot = WeaPlot(file_path=file_path)
wea_opt_plot.update_and_mse_curves_wea(start_point, expect_centers_all_f)
wea_opt_plot.param_iter_wea()
"""Power Special Case"""
wea_opt_plot.center_power_distribution()
"""Multiuple Expansion Order Case"""
files_path: list[str] = [r,r,r]
wea_opt_plot = WeaPlot(file_path=files_path)
orders: list[float] = [ , , ]
wea_opt_plot.center_comparison_with_sources(orders=orders)
```

## Wea Customized– Code Example

```
"""---WEA Method Plot Example---"""
"""--Customized--"""
"""One Expansion Order Case"""
file_path: str = r
wea_cust_plot = WeaPlot()
wea_cust_plot.customised_cost_function(file_path=file_path, standard="error")
```

|              | Source Position/mm | Latency/ms           | SNR/dB                                  |
|--------------|--------------------|----------------------|---|
| Delay Method | (58.8,0.01,183.2)  | 1.69                 | 20                                      |
|              | LMS Update Step    | LMS Iteration Number | Measurement Type                        |
| Delay Method | (10,10,10,0.001)   | 10,000               | 6 on axis<br>10/20 random on a cylinder |

Table 3: Experiment setup and the localization results of the simulated noised monopole.

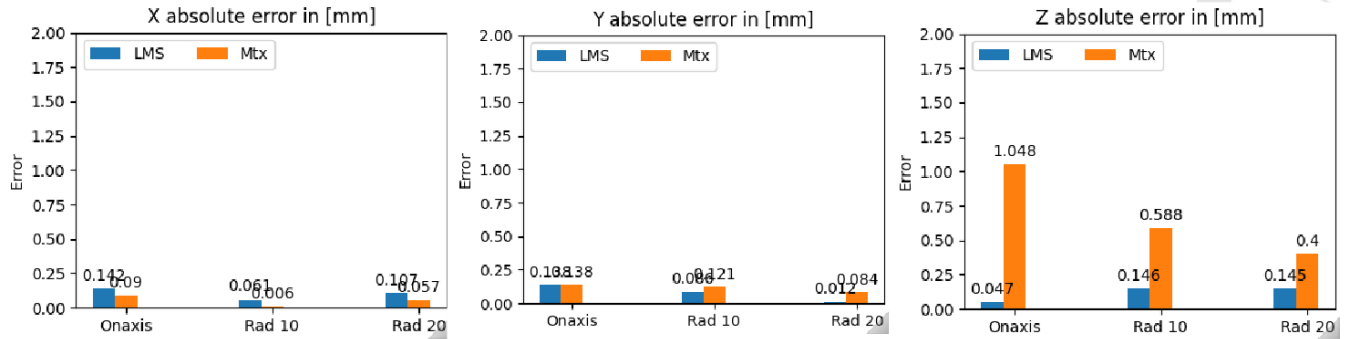


Figure 33: Absolute error results for different coordinates between the LMS and DALM algorithms for the simulated noise monopole source with 20 random points on a cylinder measurement.

## C JBL Control 1 Pro Brochure



## DETAILS

Legendary JBL Professional performance housed in a compact form-factor; the Control 1 Pro features a professional crossover network coupled with professional drivers making it ideal for even the most demanding near-field audio applications. The Control 1 Pro's updated crossover network design provides steeper crossover slopes for exceptional sonic performance and improved consistency throughout the listening area. The included wall-mount bracket enables the unit to be secured against a wall or other flat surface. Moreover, the rugged molded enclosure houses magnetically shielded transducers, making the Control 1 Pro well-suited for use with video and computer monitors, or other magnetically sensitive equipment.

## SPECIFICATIONS

### SYSTEM

- Frequency Range (-10 dB): 80 Hz - 20 kHz
- Frequency Response (+/- 3 dB): 100 Hz - 18 kHz
- Power Capacity: 150 W
- Sensitivity: 87 dB SPL, 1 W 1 m (3.3 ft)
- Maximum SPL: 108 dB continuous, 114 dB peak
- Directivity Factor (Q): 6.0
- Directivity Index (DI): 7.8 dB
- Nominal Impedance: 4 ohms
- Crossover Frequency: 4.2 kHz
- Overload Protection: Full-range SonicGuard™ power limiting to protect network and transducers.

### TRANSDUCERS

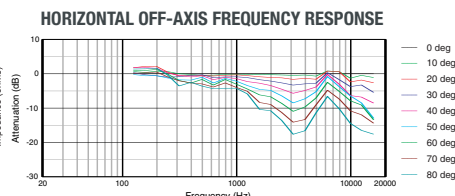
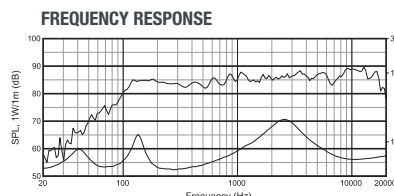
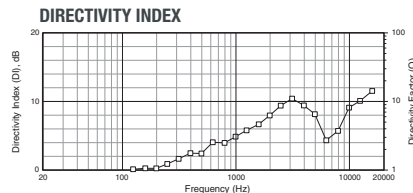
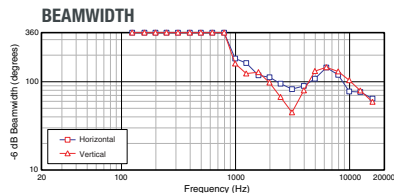
- LF Driver: 135 mm (5.25 in) low frequency loudspeaker
- HF Driver: 19 mm (.75 in) polycarbonate dome tweeter

### ENCLOSURE

- Enclosure Material: Polypropylene Structural Foam
- Finish: Black (C1Pro) or White (C1Pro-WH)
- Input Connectors: Spring-loaded terminals
- Dimensions: 235 mm x 159 mm x 143 mm (9.3 in x 6.3 in x 5.6 in)
- Net Weight (each): 1.8 kg (4 lb)
- Shipping Weight (pair): 4.6 kg (10 lb)

### ACCESSORIES

- Mounting Bracket Included
- MTC-1A ultra-duty mounting bracket (optional)
- MTC-8 heavy-duty mounting bracket (optional)



DATA C1Pro 09/06 5K

Figure 34: JBL Control 1 Pro Brochure